MATHEMATICAL MODELING OF HUMAN FACIAL MUSCLES

DİDEM AĞDOĞAN
B.S., Computer Engineering, IŞIK UNIVERSITY, 2012

Submitted to the Graduate School of Science and Engineering
in partial fulfillment of the requirements for the degree of
Master of Science
in
Computer Engineering

IŞIK UNIVERSITY
May 2015

IŞIK UNIVERSITY
GRADUATE SCHOOL OF SCIENCE AND ENGINEERING

MATHEMATICAL MODELING OF HUMAN FACIAL MUSCLES

DIDEM AĞDOĞAN

APPROVED BY:

Doç. Dr. M.Taner Eskil (Thesis Supervisor)	Işık University	_____
Doç. Dr. Olcay Taner Yıldız	Işık University	_____
Doç. Dr. Devrim Akça	Işık University	_____

APPROVAL DATE: ..../..../....

Mathematical Modeling Of Human Facial Muscles

Abstract

In this study; a new muscle model is proposed for computation of actual muscle forces that exist during facial expressions. Modeling of facial muscle forces is done on the expression of surprise. We choose this expression as it is performed by the activation of a single(frontalis) muscle. Videos used in the study are recorded with a high resolution camera where the subject's face was painted with a rectangular grid. The first and last frames of subject's surprise expression is used for extraction of muscle forces. Feature points which are located in the first frame are manually marked on the last frame with guidance of the rectangular grid. Muscle forces that are exerted on the facial skin are computed using a mass-spring model and an anatomical muscle model is derived. Skin is also modelled as a nonlinear deformable tissue for more realistic results. The accuracy of the proposed model is shown through simulations.

Keywords: facial expression, anatomical muscle model, nonlinear skin model, HIGEM, mass-spring model, simulation

İnsan Yüz Kaslarının Matematiksel Modellenmesi

Özet

Bu çalışmada mimik hareketleri sonuçunda oluşan kas kuvvetleri için yeni bir model tanımlanması yapılmıştır. Bu yaklaşımda model çıkarımı sürpriz ifadesi kullanılarak yapılır. Bunun sebebi; sürpriz ifadesinin tek bir kas (alın kası) hareketine bağlı olmasıdır. Çalışmada kullanılan videolar yüksek çözünürlüklü bir kamera ile çekilmiştir ve deneklerin yüzleri ızgara şeklinde çizilmiştir. Deneğin sürpriz yaptığı videonun ilk ve son çerçevesi kullanılır ve ilk çerçevede önceden belirlenen nirengi noktalarının son çerçevedeki yerleri yüzdeki çizgilerin yardımıyla elle belirlenir. Nirengi noktaların yer değişim sonuçunda deriye uyguladıları kas kuvvetleri bir kütle-yay modeli kullanılarak hesaplanır ve model çıkarımı yapılır. Elde ettiğimiz kas modelinin daha gerçekci olması için derinin doğrusal olmayan direnci de göz önüne alınmıştır. Bu çıkarımların sonuçunda simülasyon yapılarak önerilen modellerin doğruluğu ve gerçeğe yakın sonuçlar verdiği gösterilmiştir.

Keywords: yüz ifadeleri, anatomik kas modeli, doğrusal olmayan deri modeli, HIGEM, kütle-yay modeli, simülasyon

Acknowledgements

First and foremost I offer my sincerest gratitude to my supervisor, Doç. Dr. M. Taner Eskil, who has supported me throughout my thesis with his patience and knowledge. I attribute the level of my Masters degree to his encouragement and effort and without him this thesis, too, would not have been completed or written. One simply could not wish for a better or friendlier supervisor.

Besides my advisor, I would like to thank to Dr. Kristin Benli, for her motivation, fellowship and enormous support throughout my graduate studies.

Most importantly, none of this would have been possible without the love and patience of my family for giving birth to me at the first place and supporting me spiritually throughout my life.

Finally, I thank to my friend Elin Ehsani who accept to be a model in this study. I would like to thank Onur Görgün, who as a good friend, was always willing to help and give his best suggestions.

to My Family...
Selvi, İbrahim and Sidal . . .

Table of Contents

List of Tables

List of Figures

List of Abbreviations

2-D	**2** **D**imension
3-D	**3** **D**imension
AAM	**A**ctive **A**ppearance **M**odel
AU	**A**ction **U**nit
FACS	**F**acial **A**ction **C**oding **S**ystem
HIGEM	**HI**gh polygon **GE**neric **M**odel
NNWA	**N**earest **N**eighbor **W**eighted **A**verage
MSD	**M**ass **S**pring **D**amper
ER	**E**dge **R**epulsion

Chapter 1

Introduction

We express ourselves through verbal and non-verbal communication means. Verbal communication is through the use of words and it is the most frequently used mode of information exchange across individuals. Non-verbal communication often helps convey our unspoken feelings. One of the modes of non-verbal communication is the gestures of the body. Crossed arms on chest for defensiveness, stroking chin for trying to make a decision are a few examples that we use to express our state of mind. Facial expressions, a considerable part of non-verbal communication, constitute an integral part of interaction especially in face to face communication. Expressions provide a context for our speech by indicating both the nature and extent of our attention and meaning. In fact, it has been reported that facial expressions account for 55% of the information content of unspoken messages [1]. When we try to get our emotions, desires and our senses across the other person, we usually make use of our facial expressions. We frown when we get angry; raise our eyebrows when we are surprised, and smile when we are happy. Curiously, we perform most of these expressions unintentionally.

Research on facial expressions has a history that spans over centuries. One of the earliest known studies in this field was done by John Bulwer [2] in 1648. In his study Bulwer hypothesized that the motions of the mind and muscles of the head are directly linked, and established the muscular basis of facial expressions. In 1862, the famous neurologist Duchenne de Boulogne [3] studied generation of

facial expressions through electrical stimulation of facial muscles on live subjects. Ten years later, Charles Darwin [4] postulated that six facial expressions are common across all human cultures. He identified anger, fear, happiness, sadness, disgust and surprise as universal facial expressions.

Mechanism of facial expressions stayed solely in the research interests of psychologists until Ekman's pioneering study in 1976 [5]. Ekman defined basis functions which he termed as *action units* (AUs) that compose facial expressions. This work describes the comprehensive *facial action coding system* (FACS) for identifying the existence and strength of these basis functions. FACS defines the movement of the facial muscles, tongue and mandible via 44 different action units (AU). Ekman defines six basic facial expressions with action units. For instance; happy expression is a combination of AU6 and AU12 and surprise expression is a combination of AU1, AU2, AU5B and AU26. This well-defined procedure to extract useful information to classify facial expressions was noticed by computer scientists in late 1990s. Since then, there have been many facial expression simulation and recognition studies in the computer science domain [6, 7].

Facial expressions are sometimes elaborate, deliberately communicating a message. It has also been demonstrated that the emotional state is often involuntarily cued in facial expressions. Whether deliberate or involuntary, recognition and correct interpretation of facial expressions have important implications in many fields such as avatar generation, fatigue detection, Human Computer Interaction (HCI) applications, and game industry.

Computer scientists are continuing research on facial expressions in two fronts; simulation and recognition. In both subdomains, prior information on human face is embedded in a face model. The face, which is a non-rigid and deformable structure, is a sophisticated region of the body. The transferral of the face to a computing environment is difficult due to these characteristics of the facial structures. Model based approach defines a parametric deformable model of the

human face, that is often iteratively customized for a subject for 3D orientation, shape, and discriminative features [7–9]. An anatomically accurate generic model of human face is extremely useful for both facial expression simulation and recognition, particularly when the synthesis or analysis depends upon physical effects of facial muscles. Availability of such anatomy based models allows simultaneous analysis of real expressions on video and synthesis or mimicking on virtual characters.

Facial expression simulations are used in many different areas. The challenging tasks of simulation is to create an accurate model of the human face to be realistic. For example; as shown in the figure 1.1(left), Tin Toy (1988) created by Pixar, doesn't seem to be a real baby. The chiselled facial features gave him a scary look. Figure 1.1(middle) (Pixar-2012) reflects reality better compared to the first picture. When we look at the previous technology, we can see that facial expressions of old animation characters lack reality. Today, we get better results even if human facial expressions created by computers don't seem one hundred percent real. Another simulation example which uses facial expressions in the computer field is games. Facial expressions of characters in computer games is important to be realistic in terms of quality of the game. Popular computer games are football games such as FIFA and PES. In figure 1.1(right), we can see that the front player's face has an expression of concern. Other examples where facial expressions are used are smart phones, Speaktoit Assistant and movies.

Research on facial recognition has been carried out by scientists in the computer domain over centuries. Today, in our life, we encounter face recognition in many industrial areas. For example; digital photo camera uses facial recognition system, this camera detects smile to takes photograph automatically (Figure 1.2). Also, face recognition is used for security in many ways. For example, access can be granted through biometric properties of the face in smart homes, criminals can

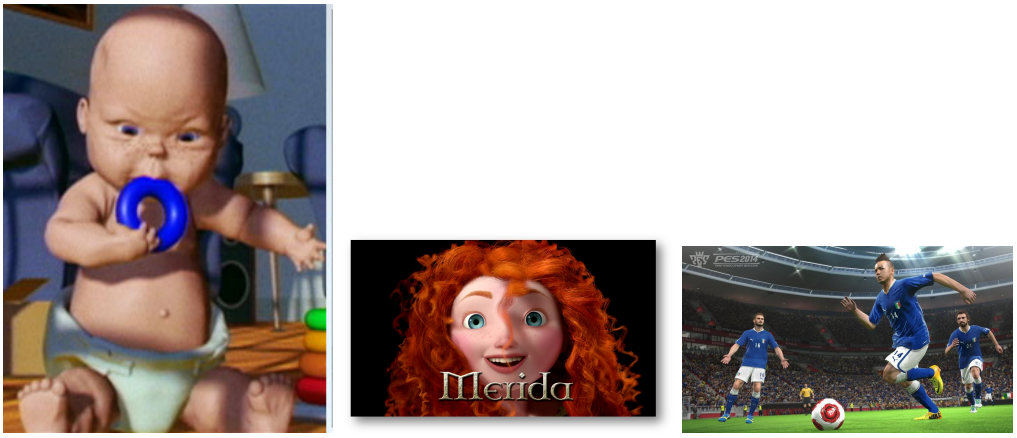

Figure 1.1: Pixar1988, Pixar2012, PES2014

be identified during investigations and personnel's entry and exit times can be tracked.

Figure 1.2: Digital photo camera with a facial expression detection module

Human face is composed of three layers which are skin layer, bone and muscle. Skin layer serves as protective clothing. The shape of one's face is delineated by the bone structure. Muscle layers are an important tissue in providing elasticity to the face. Muscles of the face lie closely underneath the skin and have a great influence on the shape and appearance of the surface. In the human face, 3 types of muscles exist; sheet, linear and sphincter. Sphincters are around mouth, eyes and nostrils; linear muscles raise the mouth corner and sheet muscles raise the middle portion of the eyebrows. Sheet muscles are planar structures and can be observed on the forehead. All facial expression are performed through

activation of facial muscles. Human face conveys thousands of different messages through contraction of facial in muscles in varying degrees and combinations. For example, Frontalis major (Figure 1.3) is triggered by surprise. Some expressions are generated with the compound effect of multiple muscles. An example to compound expressions is happiness, which consists of combination zygomaticus major and orbicularis oris.

Figure 1.3: The Frontalis muscle and surprise expression

The geometric representation of the facial model is a non-uniform mesh of polyhedral elements. To demonstrate facial expressions, face can be modelled by approximating the surface of the human face via polygons. The challenge here is the number of polygons used in the face model. Using a very large number of polygons in the construction of the face model provides more details and realism. However, the time spent on calculations gets longer. If the number of polygons is less, we can not get a detailed result. For this reason, according to the case to be done the number of polygons is determined. Realism is important for recognition and animation; it is important to have more details and resolution. For our research, we chose HIGEM face model which is moderately detailed. (HIGEM model will be explained in detail in Chapter 4).

It has been possible to obtain realistic models of human face through stereo vision [10], laser triangulation [11] and structured lighting [12]. MRI scans provide minute details on all layers of the face including the skull, muscles and the skin [13]. We therefore have extremely detailed models of the *observable* characteristics

of the human face. On the other hand, we have far less information on the inner workings of muscles and skin, which constitute the basis for all facial expressions.

An anatomically accurate muscle model should embed muscle force distribution on the skin conforming with the physical reality of spreading muscle fibers beneath a region of influence. The first muscle model was proposed by Waters [14] in 1987. Koch et al. [15] proposed a variation of this model in 1998 (In Chapter 3; these two models will be elucidated). Many model based simulation and recognition approaches implement variations of these models [12, 16–22]. Current muscle models in these two domains are built through trial and error from the model to expressions with the aim of producing more realistic simulations, i.e. they do not necessarily conform with the physical characteristics of muscles.

The best way to discover the actual muscle forces during generation of an expression would be directly probing the facial muscles. However, this is only possible through the use of intrusive sensors such as electromyograph (EMG), which adversely affect the dynamics of facial expressions. In this report, we show that unintrusive discovery of facial muscle activations through observation is in fact possible.

We solve actual muscle forces that constitute an expression solely through observation of facial deformations. We utilize a realistic face model and facial expression videos to determine the actual muscle force distribution on the face model. We exploit this distribution to derive a muscle model that reflects the physical characteristics of facial muscles. Comparative evaluation of our muscle model with the state-of-the-art reveals that the proposed model conforms better with the actual muscle forces.

In this research, we are introducing a novel muscle model that conforms to the anatomical structure of the human face. Also, we verify the accuracy of the new muscle model through simulations. We can say that, this new muscle model

is more suitable and anatomically accurate model which is customizable to any human subject.

In our study, we are using videos as input. In our videos the subjects' faces are painted with grids and they perform facial expression as instructed. In the first frame, coordinate points of specified vertices are determined. Vertices which are specified in the first frame are used to estimate the amount of displacement in the final frame. The distribution of forces is represented as vectors on the facial skin. A mathematical model for the facial muscles can be extracted from the distribution of forces on the face.

The rest of this report is organized as follows: In Chapter 2, it will provide an in-depth review on anatomy of skin and muscle structure. Chapter 3 provides information on muscle models and the face model. In Chapter 4, we review relevant previous work. In Chapter 5, we will explain the implementation of our proposed techniques. Finally, in Chapter 6, conclusions are given.

Chapter 2

Literature Survey

2.1 Biomechanics of Skin

The soft tissue of the skin is viscoelastic in its responses to stress and strain. The elastic nature of soft tissue refers to its storage of energy and tendency to return to its rest shape when the load is removed. The relation between load and deformation is non-linear. Figure 2.1 depicts relationship between stress and strain in soft tissue which are typical under uniaxial tension [23]. Under low stress, skin tissue offers very low resistance to stretch, however under greater stress it resists much more markedly. The stage of strain affects stress, which is stress-strain relation in the loading and unloading processes are different.

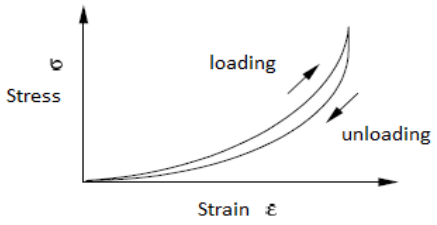

Figure 2.1: Stress-strain relationship of facial tissue [23]

Human skin has a multicomponent micro-structure. Different muscle groups are activated by the result of mimic movement of the face. This means that different forces occur in different parts of the face. Thus skin plays a major role in defining

the model. In this study, we use the nonlinear model as depicted in Figure 2.2 but approximate it using piecewise linear functions as shown in Figure 5.2.

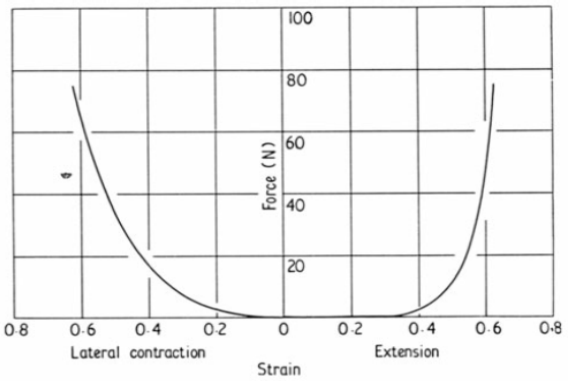

Figure 2.2: Empirical stress-strain data for facial skin [24]

2.2 Muscle Structure

All muscles consist of a bundle of fibers. The function of muscles is to produce force and motion. They are primarily responsible for maintaining and changing posture, locomotion, as well as movement of internal organs. Muscle cells contain protein filaments of actin and myosin that slide past one another, producing a contraction that changes both the length and the shape of the cell.

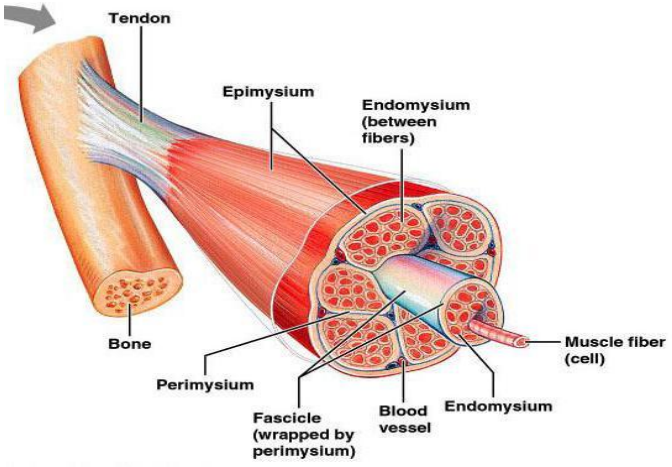

Figure 2.3: Structure of a muscle fibre

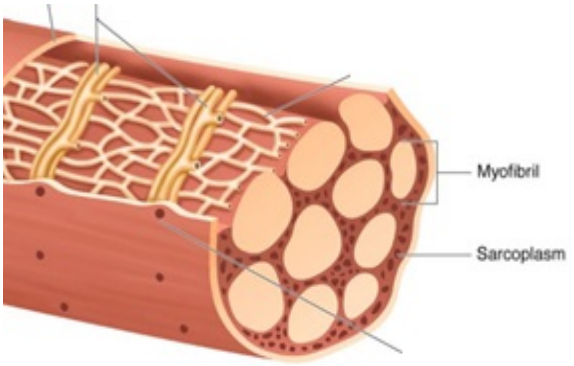

Figure 2.4: Closer view of the muscle fibre

As seen the Figure 2.3; muscle cells which are called fascicle are located throughout muscle as bundles. Each fascicle is covered with a connective tissue which is called perimysium, and this tissue holds together the muscle cells. Muscle covered with a connective tissue called fascia is formed by fascicle. Each muscle cells (muscle fibers)[Figure 2.4] has the structure of myofibrils. Myofibrils also consist of smaller units called sarcomeres.

Muscles are fiber structures that can only contract, producing pulling forces on the attached skin. The attachment of a muscle to the skin is not a single spot but a region. This is the region of influence, where the muscular force is distributed in varying intensities. Human face is often modelled through a wireframe, and the muscle-skin connection points and directions of the muscles are marked in accordance with the facial anatomy.

There are two types of muscles on the human skull; muscles of mastication and muscles of expressions. Muscle of mastication primarily deal with the movement of lower jaw and are used in mouth movements. Muscles of expressions deal with generating expressions such as happiness and anger.

Chapter 3

Muscle Model

3.1 Waters' Muscle Model

Waters' muscle model is a generic model which is proposed for creation of primary facial expressions [14]. This model is defined by small number of parameters. A muscle has a region of influence. Contraction of a muscle affects all vertices which lie in this region of influence. The distribution of exerted muscle force varies in this area. The attachment point on the skull has zero muscle force while the maximum value of muscle force is observed at the insertion point on the face. Consequently, the exerted muscle force on the vertices increases from attachment point to insertion point. Waters' linear and sheet muscle models will be explained below.

3.1.1 Linear Muscle Model

Linear muscle consists of a bundle of fibres that share a common emerging point in bone and pull in an angular direction. One of the examples is the zygomaticus major which attaches to and raises the mouth corner.

Waters defines muscles as linear springs with distributed forces in their regions of influence as shown in Figure 3.1. Contraction of a muscle affects all vertices

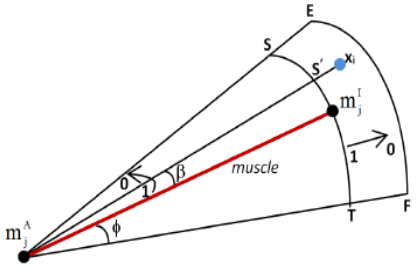

Figure 3.1: Waters' Linear Muscle Model

of the wireframe model that fall in this bounded region. Each muscle has an attachment point which is stationary point i that connects the muscle with the facial bones and an insertion point, non-stationary point, j that connects muscle with the skin of the face;

x_i : arbitrary surface point i at the face
m_j^I : insertion point of muscle j beneath the skin
m_j^A : origin of muscle j at the skull

In vector notation, we denote a fiber muscle with $\mathbf{m}_j$ and define it as;

$$\mathbf{m_j} = (m_j^A - m_j^I) \tag{3.1}$$

In Figure 3.1, x_i is any wireframe vertex, β is the angle of deviation from the fiber, and ϕ is the angular limit for region of influence. The force exerted by the muscle on wireframe vertices is faded as the angle of deviation β approaches angular limit ϕ. On the radial axis, the muscular force increases from the origin m_j^A to insertion point m_j^I and fades back to zero in the outer band of the region.

Waters defines force fading coefficients based on the angle of deviation, the distance of vertex to the muscle attachment point and the muscle fiber length. The angular fading coefficient θ_a is computed with;

$$\cos\beta = \mathbf{m}_j \cdot (m_j^A - x_i)/||\mathbf{m}_j|| \times ||m_j^A - x_i||$$
$$\theta_a = \begin{cases} \frac{cos\beta - cos\phi}{1 - cos\phi} & \text{if } cos\beta \geq cos\phi \\ 0 & otherwise \end{cases} \tag{3.2}$$

Denoting the maximum radial distance of influence with r_{max}, the radial fading coefficient θ_r is calculated as;

$$\theta_r = \begin{cases} cos\left(\frac{||m_j|| - ||m_j^A - x_i||}{||m_j||}\frac{\pi}{2}\right) & \text{if } ||m_j^A - x_i|| \leq ||m_j|| \\ cos\left(\frac{||m_j^A - x_i|| - ||m_j||}{r_{max} - ||m_j||}\frac{\pi}{2}\right) & \text{if } ||m_j|| < ||m_j^A - x_i|| \leq r_{max} \\ 0 & otherwise \end{cases} \tag{3.3}$$

The overall fading in the region of influence is the product of angular and radial fading coefficients;

$$\theta = \theta_r \cdot \theta_a \tag{3.4}$$

The external force exerted by muscles $j = 1...N$ on vertex i is calculated by the vectorial sum of all muscle forces weighted by their fading coefficients;

$$\mathbf{f}_i = \sum_{j=1}^{N} \theta_{ji} \mathbf{f}_{ji} \tag{3.5}$$

3.1.2 Sheet Muscle Model

Sheet muscle is a broad, flat sheet of muscle fiber strands without a localized emergence point. The most obvious example is the frontalis major, which raises

the middle portion of the eyebrows. This muscle model is illustrated in Figure 3.2.

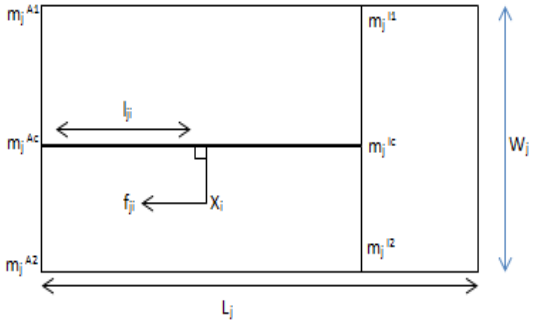

Figure 3.2: Waters' Sheet Muscle Model

Table 3.1: Sheet Muscle Model's variables

x_i:	arbitrary facial skin point
m_j^{A1} and m_j^{A2}:	attachment points defining attachment line of sheet muscle j
m_j^{Ac}:	middle point of sheet muscle attachment line
m_j^{I1} and m_j^{I2}:	insertion points defining insertion line of sheet muscle j
m_j^{Ic}:	middle point of sheet muscle insertion line
W_j:	width of rectangle zone influenced by sheet muscle
L_j:	length of rectangle zone influenced by sheet muscle
I_{ji}:	distance between x_i and sheet muscle attachment line
n_j:	constant n_j is the muscle strength factor
α_{st}:	information was not given in the article [17]

m_j^{A1} and m_j^{A2} are two points specifying the attachment line of the sheet muscle. m_j^{Ac} is the middle point of m_j^{A1} and m_j^{A2}. Similarly; the points m_j^{I1} and m_j^{I2} specify the insertion line of the sheet muscle and m_j^{Ic} is the middle point of m_j^{I1} and m_j^{I2}.

In the sheet muscle model, the muscle strength factor calculated as follows;

$$\lambda_{ji} = \frac{l_{ji}}{\parallel m_j^{Ac} - m_j^{Ic} \parallel} \tag{3.6}$$

The muscular force applied at vertex x_i is calculated as;

$$\mathbf{f}_{ji} = \alpha_{st}\theta(\lambda_{ji})\frac{m_j^{Ac} - m_j^{Ic}}{\parallel m_j^{Ac} - m_j^{Ic} \parallel} \tag{3.7}$$

$$\delta_j = \frac{L_j}{\parallel m_j^{Ac} - m_j^{Ic} \parallel} \tag{3.8}$$

$\theta(\lambda_{ji})$ changes the muscle strength according to the length factor and is defined as follows.

$$\theta(\lambda_{ji}) = \begin{cases} cos(\frac{\pi}{2}(1 - \lambda_{ji}^{n_j})) & 0 \leq \lambda_{ji} \leq 1 \\ cos(\frac{\pi}{2}(\frac{\lambda_{ji}^{n_j} - 1}{\delta_j^{n_j} - 1})) & 1 < \lambda_{ji} \leq \delta_j \\ 0 & otherwise \end{cases} \tag{3.9}$$

3.2 Koch's Muscle Model

The muscle model that belongs to Koch et al.[15] is illustrated in Figure 3.3. In this illustration, n_j^A and n_j^I are surface normals at the attachment and insertion points of muscle j, respectively.

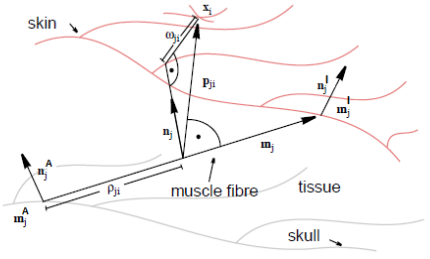

Figure 3.3: Koch's Muscle Model

The unit muscle fiber vector m_j is found as in Waters' model;

$$\mathbf{m}_{ji} = (m_j^A - m_j^I)/(\parallel m_j^A - m_j^I \parallel) \tag{3.10}$$

Koch et al. define the normal vector from a point on the muscle fiber towards the skin using the normal vectors at the attachment and insertion points of the fiber;

$$\mathbf{n}_j = (n_j^A - n_j^I)/(\parallel n_j^A - n_j^I \parallel) \tag{3.11}$$

The distance of a vertex to the muscle attachment point, projected onto the muscle fiber is denoted by ρ_{ji};

$$\rho_{ji} = (m_j^A - x_i).m_j/ \parallel m_j \parallel \tag{3.12}$$

The vector to the vertex under consideration from the closest point on the muscle fiber is found as;

$$\mathbf{p}_{ji} = (x_i - m_j^A) - \rho_{ji}\mathbf{m}_j/ \parallel m_j \parallel \tag{3.13}$$

The lateral distance ω_{ji} from the muscle fiber to the vertex is found as;

$$\omega_{ji} = \parallel \mathbf{p}_{ji} - (\mathbf{p}_{ji}.\mathbf{n}_j)\mathbf{n}_j \parallel \tag{3.14}$$

We find the ratio of the distance along the muscle fiber to the fiber length as;

$$\epsilon_{ji} = \rho_{ji}/ \parallel m_j^A - m_j^I \parallel \tag{3.15}$$

Denoting the maximum lateral distance for region of influence with ω_j, the ratio of distance of the vertex on the skin surface to the maximum lateral distance is calculated as;

$$\gamma_{ji} = \begin{cases} \frac{\omega_{ji}}{\omega_j} & \text{if } \omega_{ji} \leq \omega_j \\ \\ 1 & otherwise \end{cases} \tag{3.16}$$

Nonlinearity is introduced through sines, cosines and exponents during calculation of radial and angular fading coefficients;

$$\theta_r(\epsilon_{ji}) = sin(\frac{\pi}{2}\epsilon_{ji}^{K_j}) + \frac{1}{8}(sin(2\pi\epsilon_{ji}^{K_j} - \frac{\pi}{2}) + 1) \tag{3.17}$$

$$\theta_a(\gamma_{ji}) = \frac{1}{2}(cos(\pi\gamma_{ji}^{1.8}) + 1) \tag{3.18}$$

The exerted force by muscle j on vertex i is the product of the radial and angular fading coefficients with the unit muscle fiber vector;

$$\mathbf{f}_{ji} = \theta_r(\epsilon_{ji})\theta_a(\gamma_{ji})\mathbf{m}_{ji} \tag{3.19}$$

The resultant muscular force on vertex i is calculated by the vectorial sum of exerted forces by all muscles;

$$\mathbf{f}_i = \sum_{j=1}^{N} \mathbf{f}_{ji} \tag{3.20}$$

3.3 Face Model

Face model is needed to show the facial expression in the computer environment. Human face has a complex structure and this structure is represented as polygons or parametric surface in the computer environment. When we look at the literature, many researchers have used different face models. Some of these face

models has a simple structure while some models have a complex structure. A few examples of face models are given below.

Parke created a realistic face model by approximating the face surface with a polygonal mesh of 400 vertices and 250 polygons. Parke's model is presented in Figure 3.4.

Figure 3.4: Parke's face model

Candide is one of the well known generic face models. The original Candide model, was created by Rydfalk, contained 75 vertices and 100 triangles [25]. CANDIDE-1 which was used more frequently in the literature. This model is composed of 79 vertices and 108 surfaces. CANDIDE-2, includes 160 vertices and 238 triangles, was improved by Welsh with addition of more vertices to entirely cover the frontal head with hair, teeth and shoulders. Both models are shown in Figure 3.5.

The most recent CANDIDE model is CANDIDE-3. This version which has 113 vertices and 168 surfaces improves the rough modelling around the eyes and mouth with introduction of more vertices in these regions.

Modified [26] and multi-layered [27] versions of CANDIDE model were proposed. However, Candide is not a good candidate for precise modelling of real human

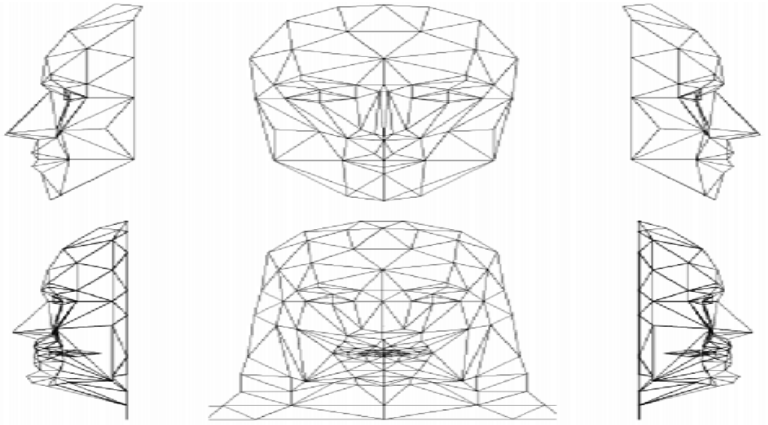

Figure 3.5: Top: CANDIDE-1 Bottom: CANDIDE-2

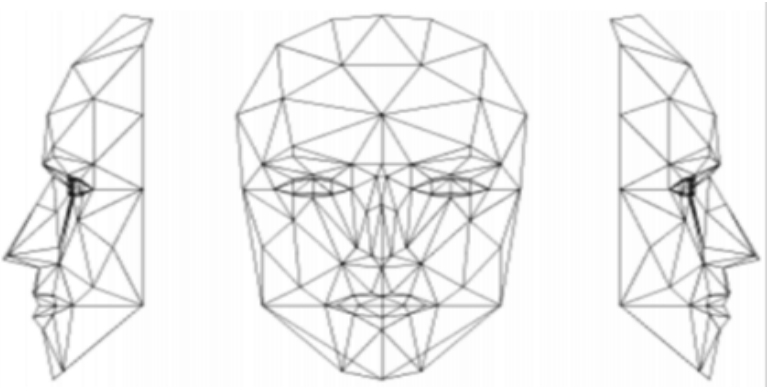

Figure 3.6: CANDIDE-3

faces. Sifakis et al. [13] built a highly detailed model that consists of 850 thousand tetrahedra in the skin layer and embeds 32 muscles.

Chapter 4

Related Work

In this chapter, we start to explain related work that is the integral part of our research. In order to extract external forces during performance of an expression, we have to customize the face model onto the subject's face, which will be introduced next. In the next step, we will introduce an inclusive face model through a wireframe. The last stage of our work is the derivation of external forces on the wireframe model.

4.1 HIGEM Model

Our face model is high polygon generic face model (HIGEM), a generic face model that conforms to the anatomy of the human face [7]. It consists of a reasonable number of vertices, a labelled set of feature points, and a realistic muscle model. The HIGEM model is presented in Figure 4.1. It comprises of 612 nodes and 1128 polygonal surfaces, which are referred to as faces in computer graphics terminology. HIGEM includes 18 major muscles of the human face (Fig. 4.2).

The wireframe is modelled as a 3D surface that is composed of polygons. Each face on the wireframe model is defined by three vertices, representing a triangular plane in the 3D space. The edges between each neighbouring vertices are modelled with springs as illustrated in Figure 4.3. In most models, muscles are defined with

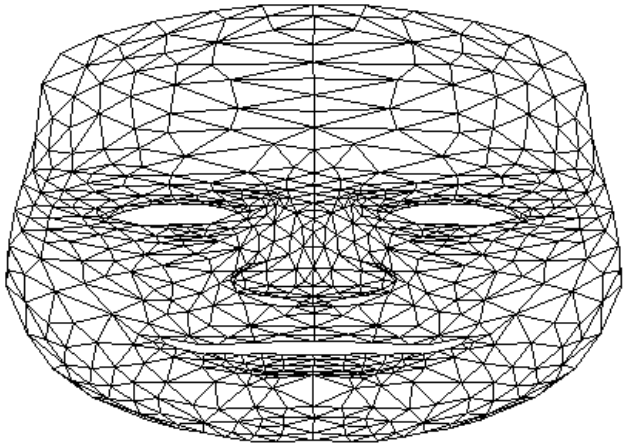

Figure 4.1: High Polygon Generic Model:HIGEM

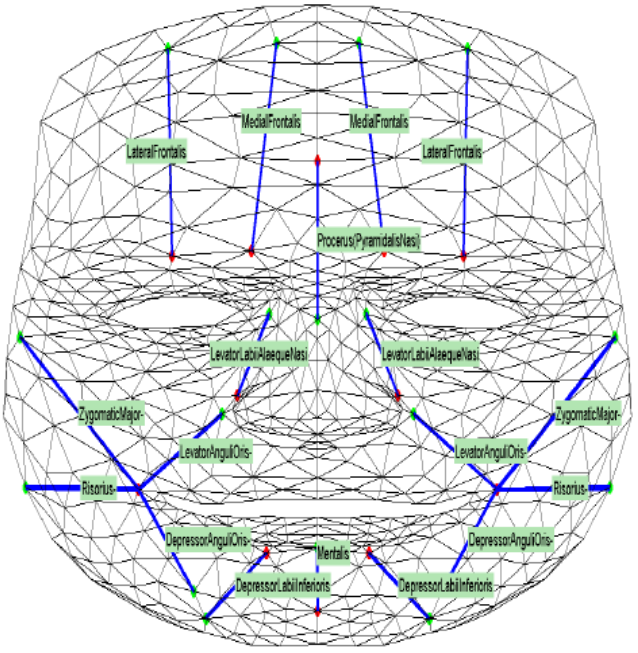

Figure 4.2: Muscles on HIGEM

attachment and insertion points on the skull and skin, respectively. Each muscle is represented by an attachment point and an insertion point, which are both denoted by wireframe vertices.

As illustrated in Figure 4.3, the edges between each neighbouring vertices are

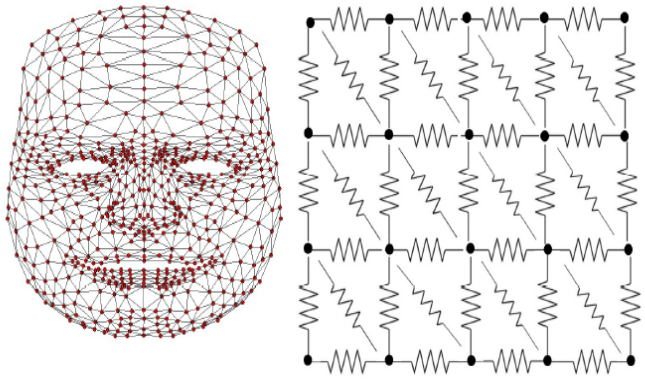

Figure 4.3: Representing the edges of the wireframe model with springs

modelled with springs. These springs represent the stiffness of the skin between neighbouring vertices.

Spring contraction between vertices i and j is composed of spring force vector on vertices i. The spring force vector on vertex i can be represented using Hooke's elasticity law;

$$\mathbf{f}_{ij} = k_{ij}(l_{ij} - \parallel x_i - x_j \parallel)\frac{x_i - x_j}{\parallel x_i - x_j \parallel} \tag{4.1}$$

The stiffness of the spring which is not fixed and will be determined using the skin model. Stiffness is denoted with k_{ij} and l_{ij} is the rest length of the spring. In above equation, the first parenthesis represents the extension or contraction magnitude of the spring. The ratio is the unit vector from x_j to x_i, which determines the direction of the spring force. We can collect the scalar terms in Eq.4.1 to obtain;

$$\begin{aligned} \mathbf{f}_{ij} &= \alpha_{ij}(x_i - x_j) \\ \alpha_{ij} &= k_{ij}\frac{l_{ij} - \parallel x_i - x_j \parallel}{\parallel x_i - x_j \parallel} \end{aligned} \tag{4.2}$$

The effective stiffness value α_{ij} depends on the displacements of vertices. α_{ij} and α_{ji} which mean mutual effective stiffness magnitudes are equal to each other. The entire model is represented with a linear set of equation, and we place the effective stiffness values for each neighbouring pairs of vertices in the stiffness matrix. If multiple springs exert force on single vertex, the effective stiffness values are summed.

An sample example is shown in figure 4.4. Without loss of generality we place the grid on a $2D$ plane, perpendicular forces can move vertices in an out of the plane. The vertices that are on the boundaries of the grid are assumed to be fixed.

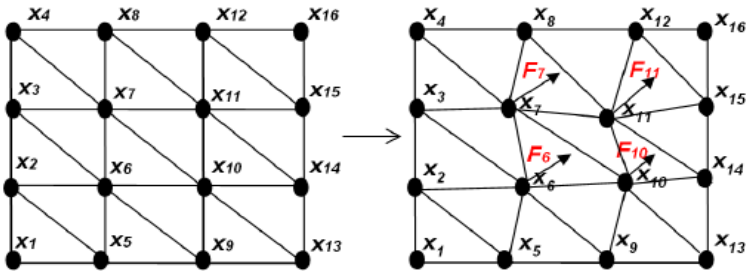

Figure 4.4: A simple wireframe model and its deformation under the influence of external forces

Vertex x_1 and both of its neighbours are fixed. There can be no extension or contraction on the attached springs. Consequently the first row of the stiffness matrix is zero. The second vertex x_2 has one neighbour x_6 which produce a spring force. The spring force on vertex x_2 by motion of x_6 is calculated with;

$$\mathbf{f}_2 = \mathbf{f}_{26} = \alpha_{26}(x_2 - x_6) \tag{4.3}$$

The second row second column become α_{26} and -α_{26} is mean second row sixth column entries of stiffness matrix K. Since there are no other internal forces on x_2, this force has to be balanced with an external force, which will appear in the second row of force matrix F.

When multiple springs exert force on a single vertex, we sum their effective stiffness values. As an example, displacement of both x_6 and x_7 may produce force on x_3 so the resultant force is computed as;

$$\begin{aligned}\mathbf{f}_3 = \mathbf{f}_{36} + \mathbf{f}_{37} &= \alpha_{36}(x_3 - x_6) + \alpha_{37}(x_3 - x_7) \\ &= (\alpha_{36} + \alpha_{37})x_3 - \alpha_{36}x_6 - \alpha_{37}x_7 \end{aligned} \tag{4.4}$$

To obtain Equation 4.4 the third row third column of the stiffness matrix to $\alpha_{36}+\alpha_{37}$. The third row sixth and seventh columns of the stiffness matrix become -α_{36} and -α_{37}, respectively.

Given the 3D coordinates of wireframe vertices and the skin model, we can calculate the stiffness matrix, which in turn will be used to determine resultant external forces on each vertex using Equation 4.5.

$$\mathbf{F} = -\mathbf{K}\mathbf{X} \tag{4.5}$$

$\mathbf{K}$ is an nxn, n is the number of vertices, matrix of stiffness values, $\mathbf{X}$ is the matrix of vertex coordinates and $\mathbf{F}$ is the resultant external forces applied on each vertex. Both $\mathbf{F}$ and $\mathbf{X}$ have n rows and 3 columns, representing the x, y and z axes.

4.2 Wireframe Customization

In this study, we use HIGEM face model which is illustrated in Figure 4.1. This model must be adapted to a human subject. We have worked with different subjects in this study such as some faces have broad forehead, the jaw of some of

them is longer or has a narrow face. For that reason, we have to customize the generic wireframe model onto the subject's face. And as the first step in, we carry out the customization once for a subject, only on first frame of the video. An inclusive face-skin model will be used to reflect facial deformations of a subject during performances of facial expression.

We use the nearest neighbour weighted average (NNWA) customization of high-polygon models [7]. NNWA has linear complexity, therefore it is the fastest possible adaptation algorithm.

Initially we selected 32 landmark vertices on the generic wireframe model for delineating the shape of the subject's face. We selected eyebrows, contours that define eyes and mouth, nose tip and nose saddles as some of our landmarks. We also identified 6 landmarks that define the contour of a face. These corresponding facial landmark points are manually marked on the first frame of the video. These correspondences will be utilized for alignment, scaling and morphing of the HIGEM model in order to customize it to the subject's face.

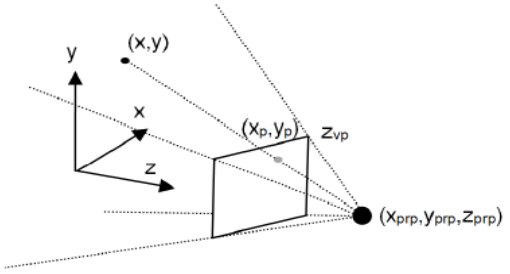

Figure 4.5: Perspective projection and ray tracing

Perspective projection is a method for mapping a $3D$ object into $2D$ camera plane is defined following. This implementation resembles the ray tracing method employed in computer graphics applications. Coordinates of the feature points in the target image x_p and y_p can be determined using perspective projection.

$$x_p = x(\frac{z_{prp} - z_{vp}}{z_{prp} - z}) + x_{prp}(\frac{z_{vp} - z}{z_{prp} - z})$$
$$y_p = y(\frac{z_{prp} - z_{vp}}{z_{prp} - z}) + y_{prp}(\frac{z_{vp} - z}{z_{prp} - z}) \tag{4.6}$$

In these equations; z_{vp} is the z-coordinate of the view plane and (x_{prp}, y_{prp}, z_{prp}) point stands for the projection reference point. We chose projection reference point on z-axis ($x_{prp} = y_{prp} = 0$) to simplify calculations;

$$\begin{aligned} f_p(x, y, z) &= (x_p, y_p) \\ &= [x(\frac{z_{prp} - z_{vp}}{z_{prp} - z}) \\ &\quad y(\frac{z_{prp} - z_{vp}}{z_{prp} - z})] \end{aligned} \tag{4.7}$$

Vertices on the wireframe model must lay on the ray that emanates from the projection reference point and passes through the facial landmark on the camera view plane, as illustrated in Figure 4.5. Keeping the depth z of the vertex fixed, we can invert using above equation to find the exact location of the vertex in $3D$ coordinate system;

$$\begin{aligned} f_p^{-1}(x_p, y_p, z) &= [x, y, z]^T \\ &= [x_p(\frac{z_{prp} - z}{z_{prp} - z_{vp}}) \\ &\quad y_p(\frac{z_{prp} - z}{z_{prp} - z_{vp}}) \\ &\quad z] \end{aligned} \tag{4.8}$$

The customization algorithm is depicted in Figure 4.6. Customization process starts by aligning and scaling the wireframe model. The initial alignment is done by positioning the generic wireframe in 3 dimensional coordinates so that the projection of the center of gravity of the model landmarks collides with that of target image.

Scaling in x, y, z axes are done separately. Scale in horizontal and vertical axes are determined from the ratio of range of projected vertices and observed facial landmarks. Since we do not have any information on the z dimension, we heuristically assume the scale factor for depth to be 1.15 times the scaling factor of the width of the head. This is performed relying on the statistics reported by Luximon [28].

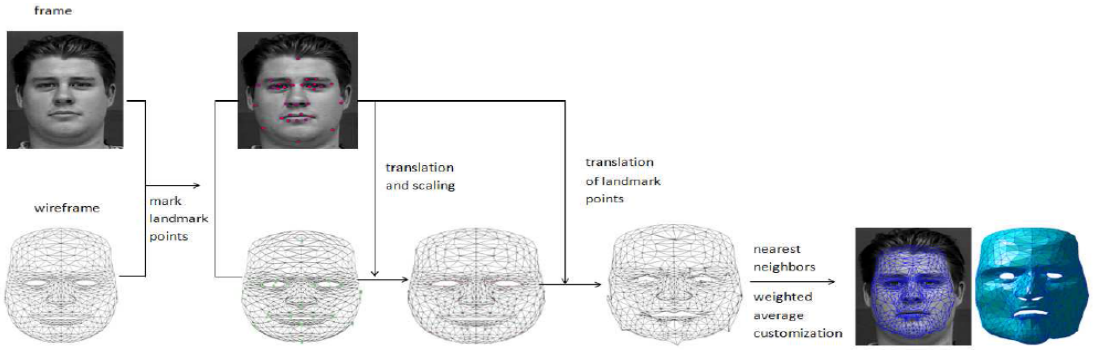

Figure 4.6: Nearest neighbor weighed average customization algorithm

We use Equation 4.7 to translate the landmark vertices of the wireframe model so that their projections coincide with facial landmarks. There are only 32 landmark vertices on the wireframe model and the remaining 576 vertices are not yet translated to match the observation. A non-landmark vertex is translated with a weighted sum of vectorial displacement of neighbouring landmark vertices, inversely weighted with its $3D$ distances to the landmarks.

4.3 Numerical Simulation of Facial Expressions

This section will explain mass-spring-damper model. The $3D$ face model used in this research is HIGEM which consists of a single layer and a set of facial muscles. HIGEM defines all major muscles that exists on human face. The face mesh is defined as a classical MSD system in which each vertex is represented with a point mass and edges connecting the neighbouring vertices are represented by springs. The viscoelastic behaviour of the skin with non linear springs connecting point masses is modelled. The structural spring force vector $\mathbf{S}_{ij}$ that is applied on vertex i by its neighbouring vertex j is defined as;

$$\mathbf{s}_{ij} = -(1 + (||\mathbf{x}_{ij}|| - d_{ij})^2)^{\gamma} \times k_0(||\mathbf{x}_{ij}|| - d_{ij}) \frac{\mathbf{x}_{ij}}{||\mathbf{x}_{ij}||} \tag{4.9}$$

where $\mathbf{x}_{ij} = x_i - x_j$ is a vector from neighbouring vertex j to vertex i, γ is the non-linearity factor and d_{ij} is the rest length of the spring.

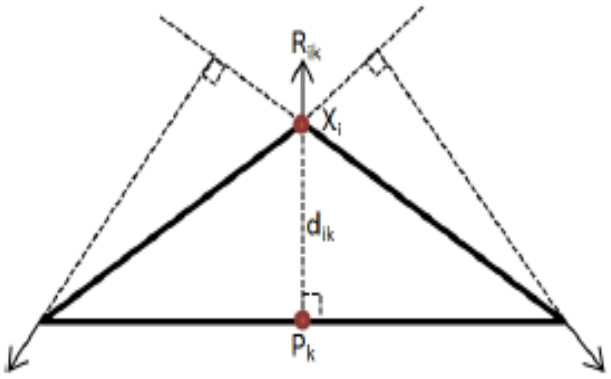

Figure 4.7: Edge repulsion forces

Cooper and Maddock expressed that the point mass can pass the opposite edge under large force and this is referred to as folding. Under strong forces, it is

possible to avoid this folding, by use of a virtual opposing force. The edge repulsion(ER) force, is based on the perpendicular distance of the point to the opposite edge and is always away from the edge, is depicted in figure 4.7. The vector of repulsive force is calculated as;

$$\mathbf{r}_{ik} = -(1 + (||x_i - p_k|| - d_{ik})^2)^{\zeta} \times k_0(||x_i - p_k|| - d_{ik})\frac{x_i - p_k}{||x_i - p_k||} \tag{4.10}$$

$\mathbf{r}_{ik}$ is a repulsive force vector which is applied to the vertex to prevent folding, p_k is the projection point of x_i onto the opposite edge, ζ is the non-linearity factor and d_{ik} is the rest length of the ER spring.

The elastic skin force is modelled with structural spring and edge repulsion forces. Damping models the viscoelastic dissipation of energy on the skin. Damping produces a force vector;

$$\mathbf{d}_i = -c\frac{dx_i}{dt} \tag{4.11}$$

where c is damping coefficient. The resultant force on a vertex is calculated as;

$$\mathbf{f}_i = \sum_{n \epsilon M} \mathbf{t}_{in} + \sum_{j \epsilon N_i} \mathbf{s}_{ij} + \sum_{k \epsilon E_i} \mathbf{r}_{ik} + \mathbf{d}_i = m\frac{d^2 x_i}{dt^2} \tag{4.12}$$

The above equation defines the dynamics of a MSD system where M is the set of muscles, N_i is the set of neighbouring vertices of i, E_i is the set of opposing edges of i and m is the point mass of the vertex. Equation 4.12 is a second order ordinary differential equation that can be solved by a numeric integrator.

The coordinate of vertex i can be estimated in the next time step $(t+1)$ for small time steps δt;

$$x_i{}^{t+1} = x_i^t + \Delta t \mathbf{v}_i^{t+1} \tag{4.13}$$

For calculation of x_i^{t+1}, the velocity vector $\mathbf{v}_i^{t+1}$ of the vertex in the next time step is estimated.

$$\mathbf{v}_i^{t+1} = \mathbf{v}_i^t + \frac{\Delta t}{m}\Big(\sum_{n\in M} \mathbf{t}_{in}^{t+1} + \sum_{j\in N_i} \mathbf{s}_{ij}^{t+1} + \sum_{k\in E_i} \mathbf{r}_{ik}^{t+1} - c\mathbf{v}_i^{t+1}\Big) \tag{4.14}$$

We collect scalar terms in Equation 4.14 and define two scalars, g_{ij} and h_{ik};

$$\begin{aligned}
g_{ij}^{t+1} &= -(1 + (||\mathbf{x}_{ij}^{t+1}|| - d_{ij})^2)^\gamma \\
&\qquad \times k_0(||\mathbf{x}_{ij}^{t+1}|| - d_{ij})\Big/||\mathbf{x}_{ij}^{t+1}|| \\
\mathbf{s}_{ij}^{t+1} &= g_{ij}^{t+1}\mathbf{x}_{ij}^{t+1} \\
h_{ik}^{t+1} &= -(1 + (||x_i^{t+1} - p_k^{t+1}|| - d_{ik})^2)^\zeta \\
&\quad \times k_0(||x_i^{t+1} - p_k^{t+1}|| - d_{ik})\Big/||x_i^{t+1} - p_k^{t+1}|| \\
\mathbf{r}_{ik}^{t+1} &= h_{ik}^{t+1}(x_i^{t+1} - p_k^{t+1})
\end{aligned} \tag{4.15}$$

Using Equations 4.13, 4.14 and 4.15 we can define next velocity as;

$$\mathbf{v}_i^{t+1} = \mathbf{v}_i^t + \frac{\Delta t}{m}\Big(\sum_{n\in M} \mathbf{t}_{in}^{t+1} + \sum_{j\in N_i} g_{ij}^{t+1}(x_i^t + \Delta t \mathbf{v}_i^{t+1} - x_j^{t+1}) + \sum_{k\in E_i} h_{ik}^{t+1}(x_i^t + \Delta t \mathbf{v}_i^{t+1} - p_k^{t+1}) - c\mathbf{v}_i^{t+1}\Big) \tag{4.16}$$

Solving Equation 4.16 for v_i^{t+1};

$$\mathbf{v}_i^{t+1} = \Big(m\mathbf{v}_i^t + \Delta t \sum_{n\in M} \mathbf{t}_{in}^{t+1} + \sum_{j\in N_i} g_{ij}^{t+1}(x_i^t - x_j^{t+1}) + \sum_{k\in E_i} h_{ik}^{t+1}(x_i^t - p_k^{t+1})\Big) \Big/ \Big(m + \Delta t c - \Delta t^2(\sum_{j\in N_i} g_{ij}^{t+1} + \sum_{k\in E_i} h_{ik}^{t+1})\Big) \tag{4.17}$$

The next velocities $\mathbf{v}_i^{t+1}$ of vertices are estimated through Equation 4.17. These estimated velocities will be used in Equation 4.13 to update vertex coordinates x_i^{t+1}.

Human face has a curved structure, because of this muscle forces can lead to skull penetration when muscle force has a component that is directed into the skin mesh.

Figure 4.8 illustrates a muscle force that could lead to the collapse of the mesh. In Erkoc's study [29]; to prevent collapse of the face model, computationally efficient

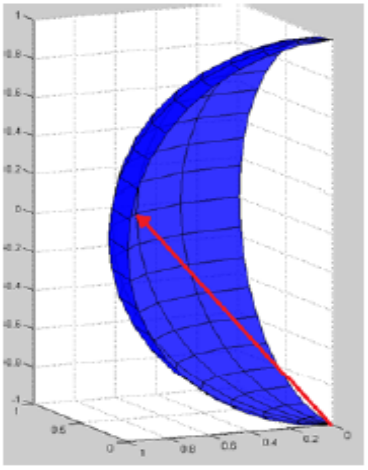

Figure 4.8: 3D muscle force direction in single layer face model

algorithm is proposed. The face model consists of a skin layer and facial muscles without represent of a skull structure.

In this algorithm, muscle forces are calculated in $2D$ space in order not to pull vertices into the mesh surface. From $3D$ to $2D$ transformation is performed as follows;

$$u = \arctan(\frac{x}{z}), \qquad v = y \tag{4.18}$$

The muscle force is calculated with Equation 4.18 in $2D$ space. The $3D$ coordinates of vertices are utilized to calculated the normal for the $3D$ surface with;

$$\mathbf{n} = (x_2 - x_1) \times (x_3 - x_1) \tag{4.19}$$

where x represents a vertex defining a triangular face in $3D$. Using the surface normal, we define the surface equation as;

$$\mathbf{n}.(x - x_1) = 0 \tag{4.20}$$

Equation 4.20 can be expanded to obtain;

$$n_x(x - x_1) + n_y(y - y_1) + n_z(z - z_1) = 0 \tag{4.21}$$

We will use this plane equation to determine the projection of the $2D$ muscle force vector to the $3D$ space. Solving Equation 4.18 for x and y, we obtain;

$$\begin{aligned} x &= z\tan(u) \\ y &= v \end{aligned} \tag{4.22}$$

Substituting Equation 4.22 into Equation 4.21 and solving for z;

$$z = \frac{n_x x_1 - n_y(v - y_1) + n_z z_1}{n_x \tan u + n_z} \tag{4.23}$$

Equations 4.22 and 4.23 give us the muscle force vector on vertex x_1 in the $3D$ coordinate system of the wireframe. This vector lies one of the faces vertex x_1 resides on. The muscle force vectors generated by the activity of Medial Frontalis muscle is depicted in Figure 4.9. Figure 4.11 provides a close up on the affected vertices.

In this model; the proposed approach uses stack structure. Calculation of muscle force distribution is started at the insertion point of the muscle, where the muscle

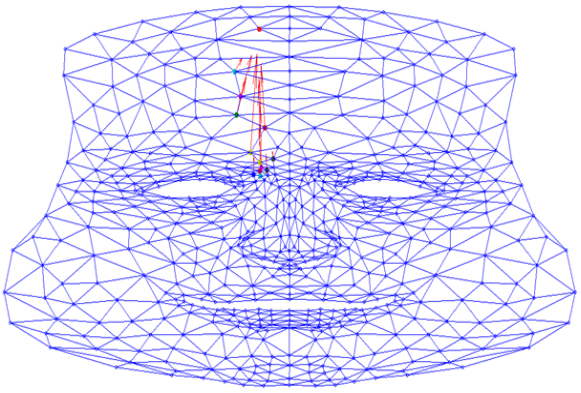

Figure 4.9: The calculated muscle forces for Medial Frontalis Muscle

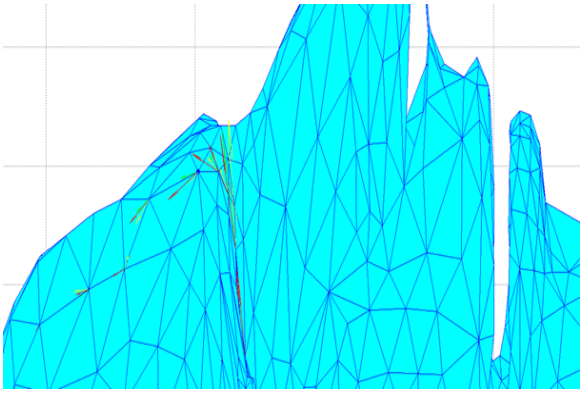

Figure 4.10: Muscle forces on $3D$ face model

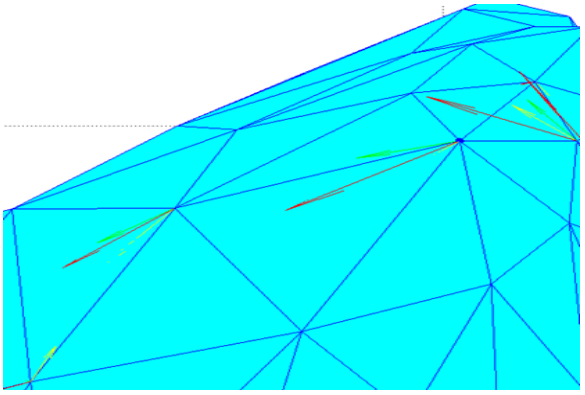

Figure 4.11: Close up of Figure 4.10

force is at its peak, by pushing that vertex onto the stack. If the calculated force on this vertex is not negligible, its direct neighbours are pushed into the stack. This procedure is repeated for each muscle, until there is no element left in the stack. Use of stack enables calculating muscle forces only for those vertices that are in the region of influence of a muscle.

Chapter 5

Proposed Model

In this research; real muscle forces are extracted on the face during performance of a facial expression. We tracked the progress of surprise expressions from different subjects using a 1036 x 1036 pixel camera. In each experiment, the subject's face was drawn a grid [Figure 5.1]. In the first frame feature points were determined and the corresponding feature points are manually marked in the last frame. Thus, this grid will be used for aid in marking of feature point coordinates. The reason of making model using surprised expression is that it is not a compound expression, i.e. it is produced by the effect of a single muscle, namely the Frontalis muscle [30]. For example, happy expression occurs under the influence of more than two muscles. This case clearly demonstrates why we choose surprised expression (These case' images are giving in appendix).

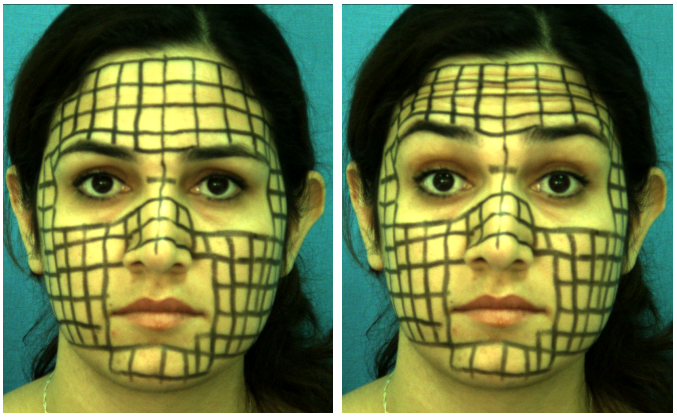

Figure 5.1: The view of subject's face in the first and last frame

External muscle forces on the wireframe vertices described in the foregoing discussion are calculated by using feature point coordinates in Equation 4.5. Muscle model is extracted from these muscle forces obtained in the forehead region and this model has been applied to other areas of the face. This model which is proposed is also used in simulation and facial analysis. Also, skin model which is represented by piecewise linear interpolation as illustrated in Figure 5.2 is used and stiffness matrix K is calculated using skin model. We will elucidate the steps of our approach in this chapter.

Initially; we will clarify the skin model which constitudes a considerable part in our model. Then; muscle model proposed will be explained in detail. Lastly, facial expression simulation results will be given.

5.1 Skin Model

Facial skin is composed of the epidermis, dermis and hypodermis layers. The biomechanical properties of living tissues have been extensively studied. The stress-strain relationship of the skin depends on the phase (load relaxation), temperature of the skin and the nature of stress such as the number of loading cycles, uniaxial an biaxial loading, etc. Fung [23] provides a constitutive expression for the skin which shows that the relationship between stress and strain is highly nonlinear. Experimental findings on biomechanics of skin lead researchers to nonlinear modeling in both facial expression simulation and recognition studies [18], [22], [31].

Figure 5.2 presents a typical stress-strain diagram for the skin [23]. The data points represent the actual measurements of force taken in positive (elongation) and negative (contraction) directions. We model this nonlinear property of the skin through piecewise linear interpolation, shown as red and blue lines overlayed

on the data points. In other words, the stiffness of the skin changes for varying magnitudes of elongation and contraction in our implementation.

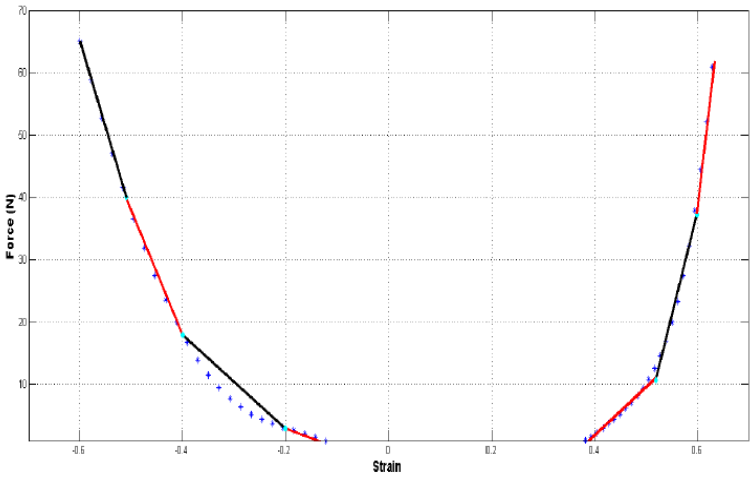

Figure 5.2: The stress-strain diagram for the skin for contraction and elongation

The Figure 5.2 is obtained from the Figure 2.2 [24] through piecewise linear interpolation. Skin model which is embedded in our implementation provided realistic results.

5.2 Muscle Model

The muscular system of the human face model is comprised of 18 muscles. They are attached with both the skull and the facial tissue. Each muscle activity is a compound effect of many fibres, this increases its influence area on the facial surface.

In our implementation, the muscle fibers are defined on the wireframe vertices which stand for skin points. We assume that the muscle fiber is beneath the skin surface at all points and the skin is infinitesimally thin. Under this assumption the skin collapses onto the skull, and lateral distance becomes the length of the vector from the nearest point on the muscle fiber to the vertex under consideration.

The following Figures 5.3 show different between Koch muscle model and proposed muscle model. Koch muscle model, Equation 3.14 which is explained in Chapter 3, defines a normal vector on the skin, however our proposed muscle model ignores the normal vector because of the thinness of the skin.

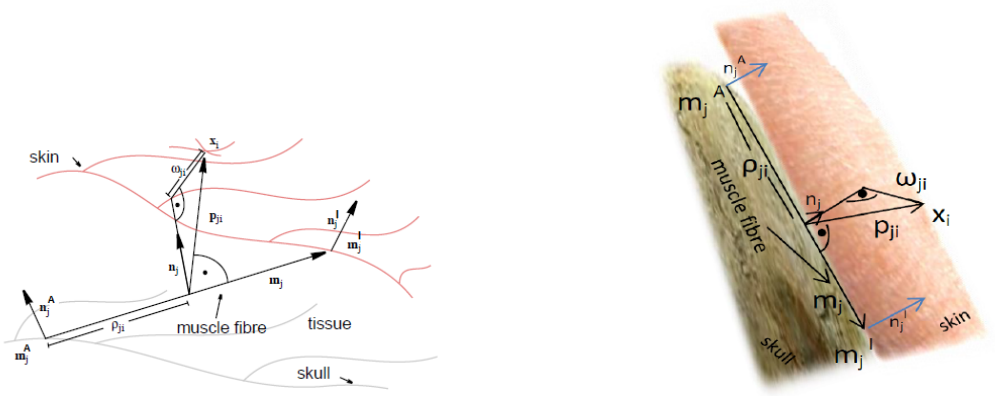

Figure 5.3: Koch Muscle Model and Our Proposed Muscle Model

Due to the differences in the Figure 5.3; Equation 5.1 will be used as a replacement of Equation 3.14 in the Chapter 3.

$$\omega_{ji} = ||p_{ji}|| \tag{5.1}$$

The remaining part explains that how we model muscle force on forehead during the performance of surprise expression. The force of each vertices on the face is calculated using Equation 4.5 as described in the Chapter 4.

In Figure 5.4, the first and last frames of the expression of surprise illustrate on the subject's face. On the first frame, the white points are the projections of vertices in the customized wireframe model in the forehead region. On the last frame, the corresponding feature points are manually marked and projected back to the wireframe. In facial expression recognition applications, these points are

tracked through image processing techniques which are optic flow and particle filtering. For our research, we manually mark the final coordinates of each white point by hand to obtain better accuracy in extraction of muscle forces.

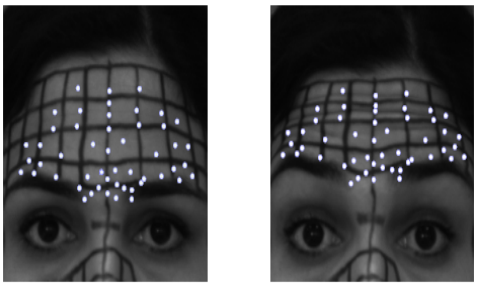

Figure 5.4: First and last frame of the surprise expression

These selected feature points which are manually marked in the last frame of the video projected back to the 3D coordinate system using Equation 4.8, and Figure 5.5 illustrates the 3D coordinates of the wireframe to reflect the deformation due to expressions on the face image.

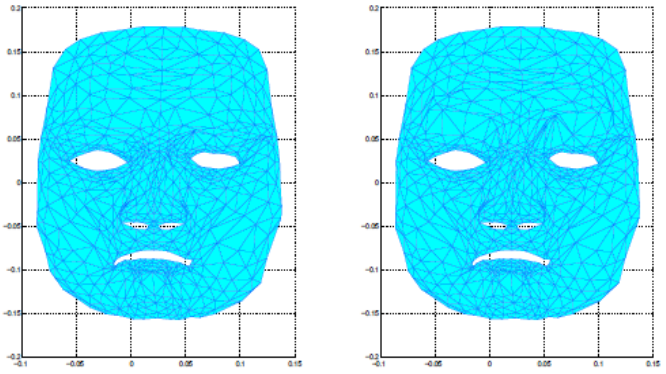

Figure 5.5: Customized wireframe and its deformation for surprise expression

The external force on the wireframe vertices are calculated by using this $\mathbf{F} = -\mathbf{KX}$ equation. $\mathbf{K}$ called stiffness matrix is calculated using the skin model and effective stiffness values. Vertex coordinate matrix $\mathbf{X}$ consist of n rows and 3 columns, representing the x, y and z axes. Note that stiffness k_{ij} depends on the stretch of the spring with respect to the piecewise linear interpolation as depicted

in Figure 5.2. Effective stiffness α_{ij} depends both on the skin stiffness and stretch as implied by;

$$f_{ij} = \alpha_{ij}(x_i - x_j)\alpha_{ij} = k_{ij}\frac{l_{ij} - \parallel x_i - x_j \parallel}{\parallel x_i - x_j \parallel} \tag{5.2}$$

The obtained distribution of external forces give us information about actual muscle force magnitudes on the forehead during the performance of surprise expression. This is illustrated in Figure 5.6. In this figure, the height of the wireframe vertices in 3D coordinate system are replaced with the magnitude of muscular force for visualization.

We observe that the distribution of actual muscle forces are nonlinear as suggested in the conventional muscle models. However, contrary to the conventional models, the region of influence of the Frontalis muscle is very narrow, and on a patch that follows the insertion points of muscle fibers to the skin. Note that Koch et al. aimed to realize this effect on the radial dimension with the nonlinearity factor K_j as in Equation 3.17. The distribution of force is also nonlinear on the angular dimension.

Observation of Figure 5.6 reveals that the general form of the muscle force distribution is an hyperbolic tangent function of strain. This nonlinear function form is found to be representative of muscle force distribution both in radial and angular dimensions. We apply nonlinear least squares to fit functions on the muscle forces that were illustrated in Figure 5.6 to obtain the anatomical muscle model as;

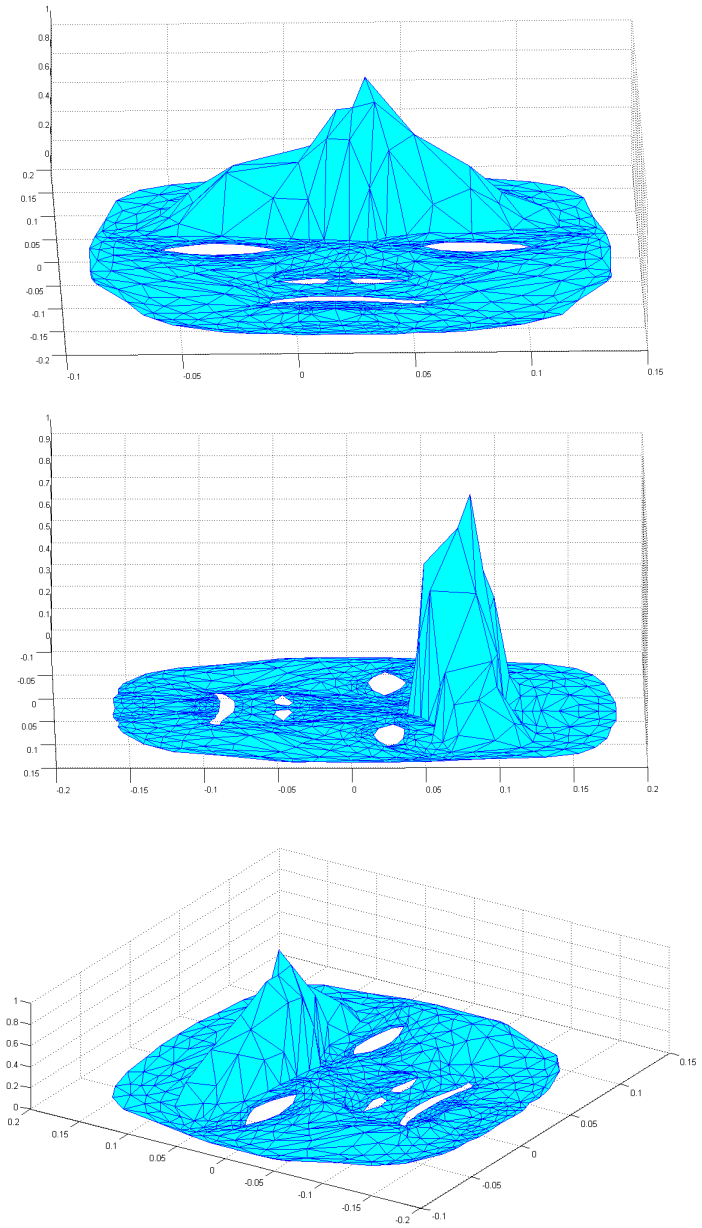

Figure 5.6: Actual muscle model magnitudes for the surprise expression

$$\theta_r(\epsilon_{ji}) = \begin{cases} (1/2)((tanh(sr * (\epsilon_{ji} + wr/2)) + 1) - (tanh(sr * (\epsilon_{ji} - wr/2)) + 1)) & \text{if } \epsilon_{ji} > 1 \\ 0 & otherwise \end{cases} \tag{5.3}$$

$$\theta_\alpha(\gamma_{ji}) = (1/2)((tanh(sa*(\gamma_{ji}+wa/2))+1)-(tanh(sa*(\gamma_{ji}-wa/2))+1)) \quad (5.4)$$

where sr and wr are the radial constants and sa and wa are the angular constants. These four constants are found using error minimization. Firstly, we obtain actual force and using Matlab *fminsearch* function. We optimize with difference between the actual force and our proposed model for this four constants. And we find the appropriate values for these four constants.

The exerted force;

$$f_{ji} = \alpha\theta_r(\epsilon_{ji})\theta_\alpha(\gamma_{ji})\mathbf{m_{ji}} \quad (5.5)$$

$\mathbf{m_{ji}}$ is defined 3.10. α is also determined appropriate values for each expressions.

$$\epsilon_{ji} = (||xa_{ji}|| * cos(\theta) - ||m_{ji}||)/||m_{ji}|| \quad (5.6)$$

$$\gamma_{ji} = ||xa_{ji}|| * sin(\theta)/||m_{ji}|| \quad (5.7)$$

$\mathbf{xa_{ji}}$ is a vector between vertex and attachment point. θ is a angle between $\mathbf{m_{ji}}$ and $\mathbf{xa_{ji}}$.

The radial and angular fading coefficients are calculated using hyperbolic tangent function, which is depicted in Figure 5.7. Note that radial distance ratio ϵ is zero and one at the attachment point to the skull and insertion point to the skin, respectively. The radial fading coefficient increases gradually starting from the attachment point and abruptly drops to zero beyond the insertion point. Similarly; the angular fading coefficient is maximum on the muscle fiber and gradually decreases as the distance of the vertex to the fiber increases. Functions

θ_r and θ_α closely follow the actual force variation (Figure 5.7) on radial and lateral cross-sections.

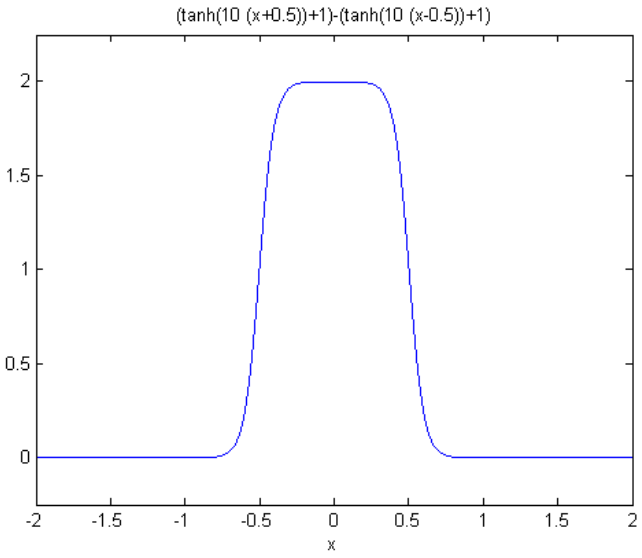

Figure 5.7: Hyperbolic tangent function for the proposed model

We applied the anatomical muscle model using the default muscles provided by HIGEM (Figure 4.1). The distribution of force magnitudes with the anatomical muscle model is illustrated in Figure 5.8. Note that actual muscle forces drop to zero abruptly around eyes since these vertices were not manually marked for displacement and were not calculated. On the other hand, muscle forces were generated for all vertices using the anatomical muscle map.

Our anatomical muscle model was derived using actual data belonging to a subject. For a fair comparison of muscle models, we chose another subject from our database, marked facial feature points on the first and last frames, and computed the actual muscle forces. The distribution of force magnitudes for the new subject is illustrated in Figure 5.9. As before, the force distribution were calculated through vertex displacements. The comparative analysis of muscle models will be carried out on this new subject. Comparing Figures 5.8 and 5.9, we observe that the anatomical muscle model produces physically realistic results.

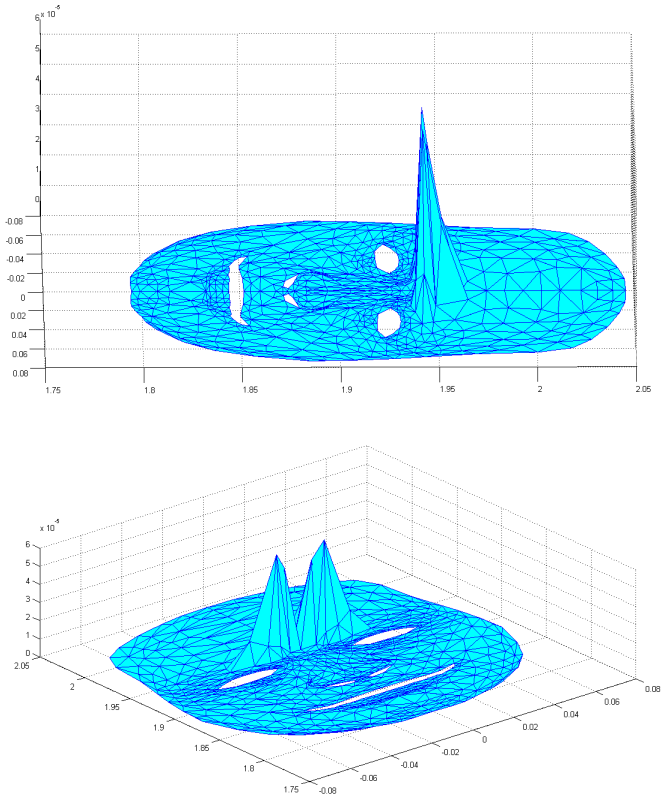

Figure 5.8: Distribution of muscle force magnitudes using anatomical muscle model

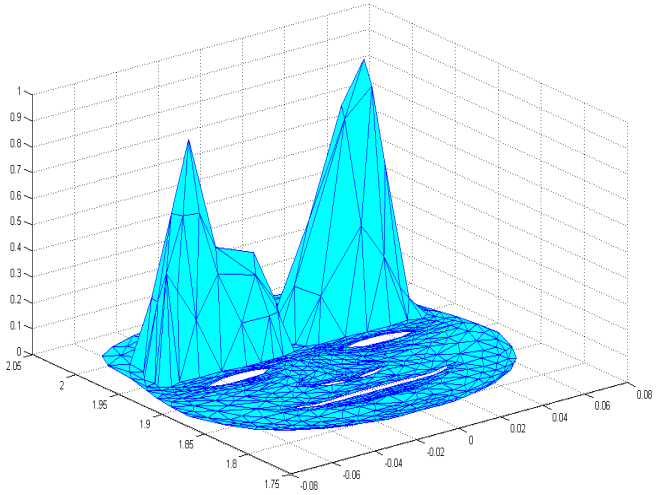

Figure 5.9: Actual muscle force magnitudes for subject 2

5.3 Simulation of Facial Expressions

Table 5.1 shows 6 facial expressions which are surprise, happy, sad, anger, disgust and fear.

Table 5.1: In order of the top down: (a)Surprise (b)Happy, (c)Sad, (c)Anger, (d)Disgust, (e)Fear

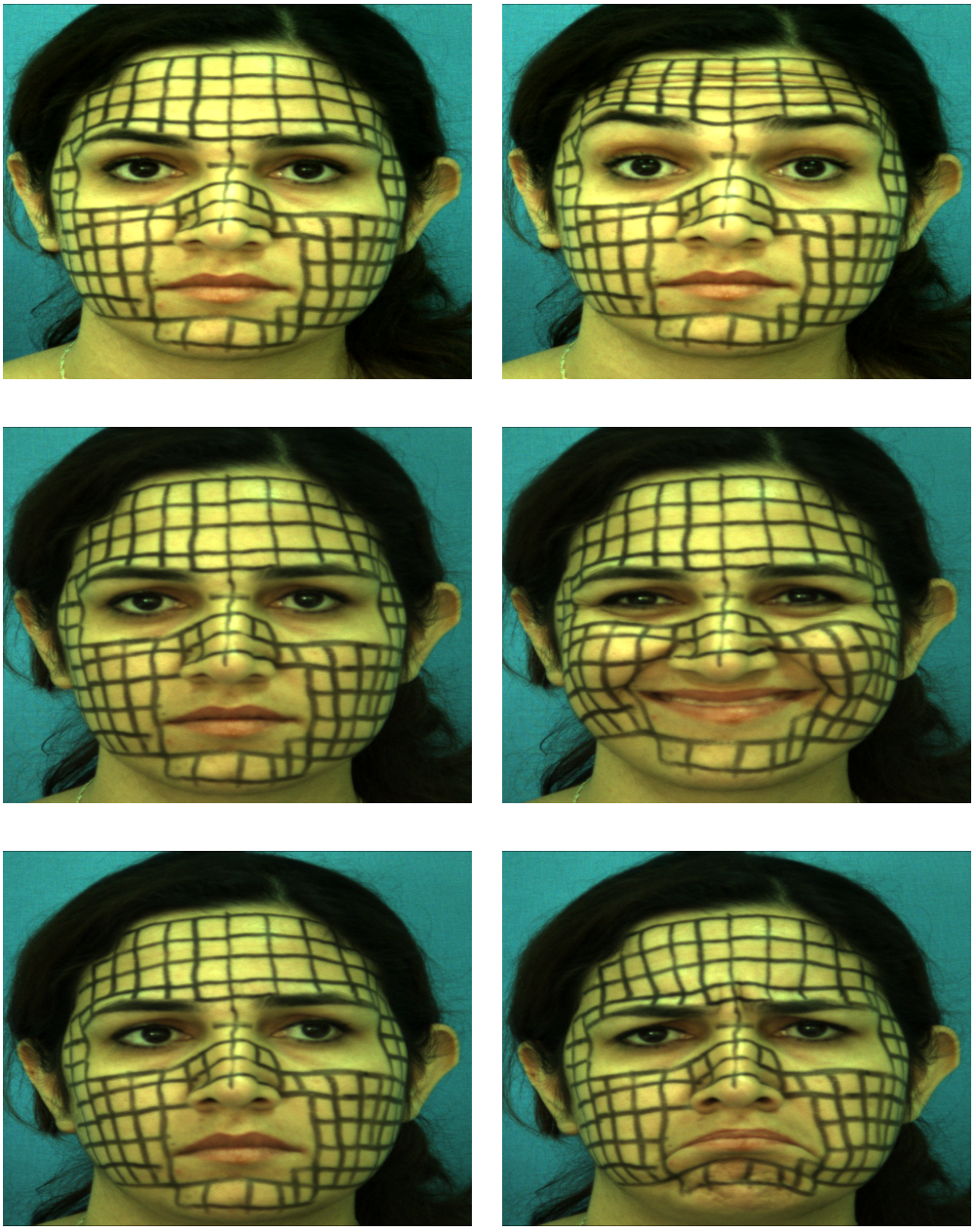

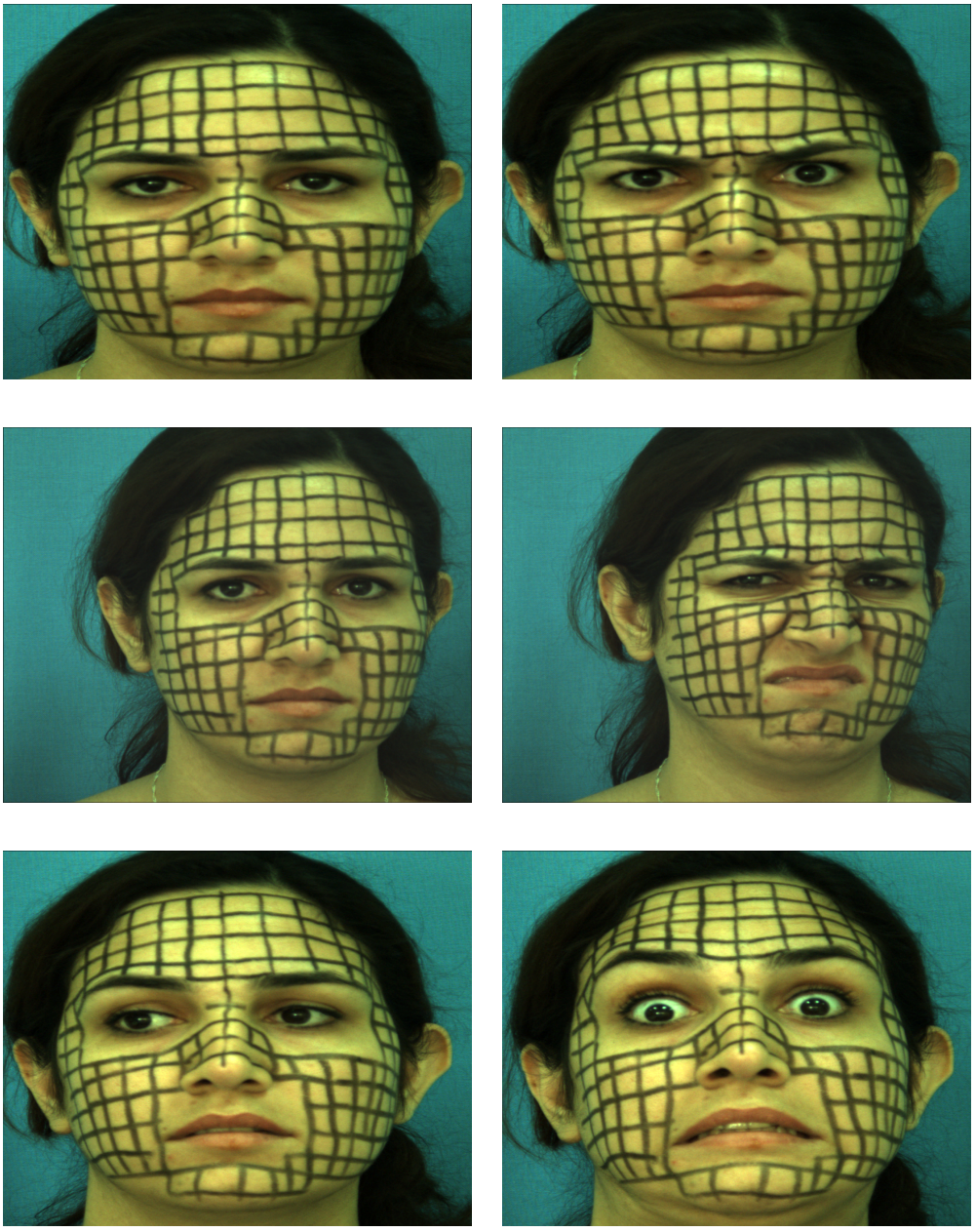

The proposed muscle model is tested with the simulation give realistic results. The first subfigure in table 5.3 shows the facial expression surprise. In this expression, the frontalis muscle is only activated.

Muscles' locations are determined based on anatomical facial model making of the simulation 5.10.

Table 5.2 shows muscles' locations for six different facial expressions.

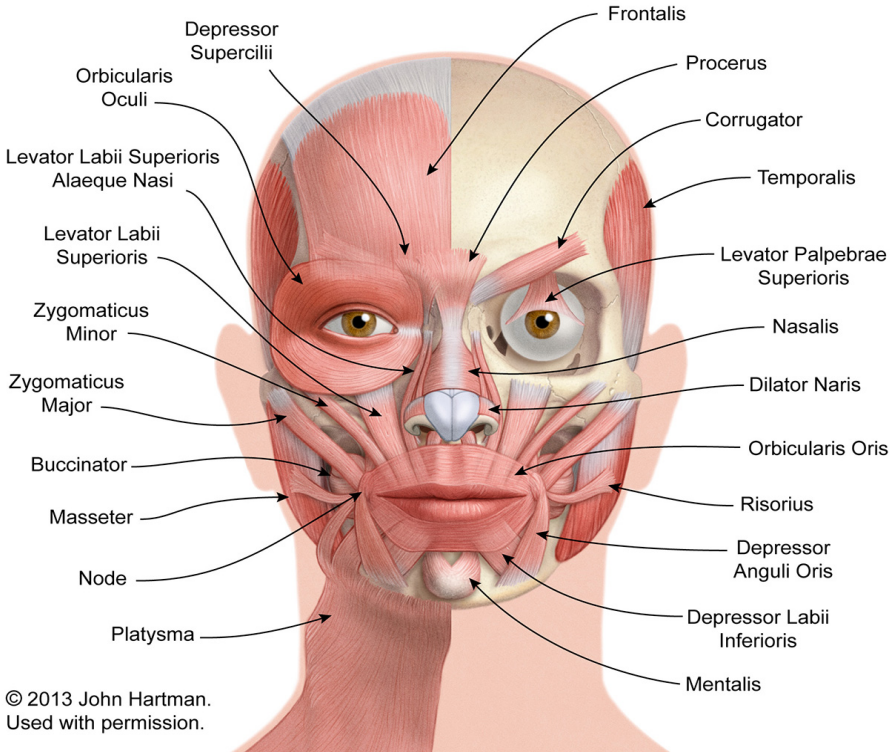

Figure 5.10: Facial Muscles Anatomy

Table 5.2: In order of the left to right: (a)Surprise (b)Happy, (c)Sad, (c)Anger, (d)Disgust, (e)Fear

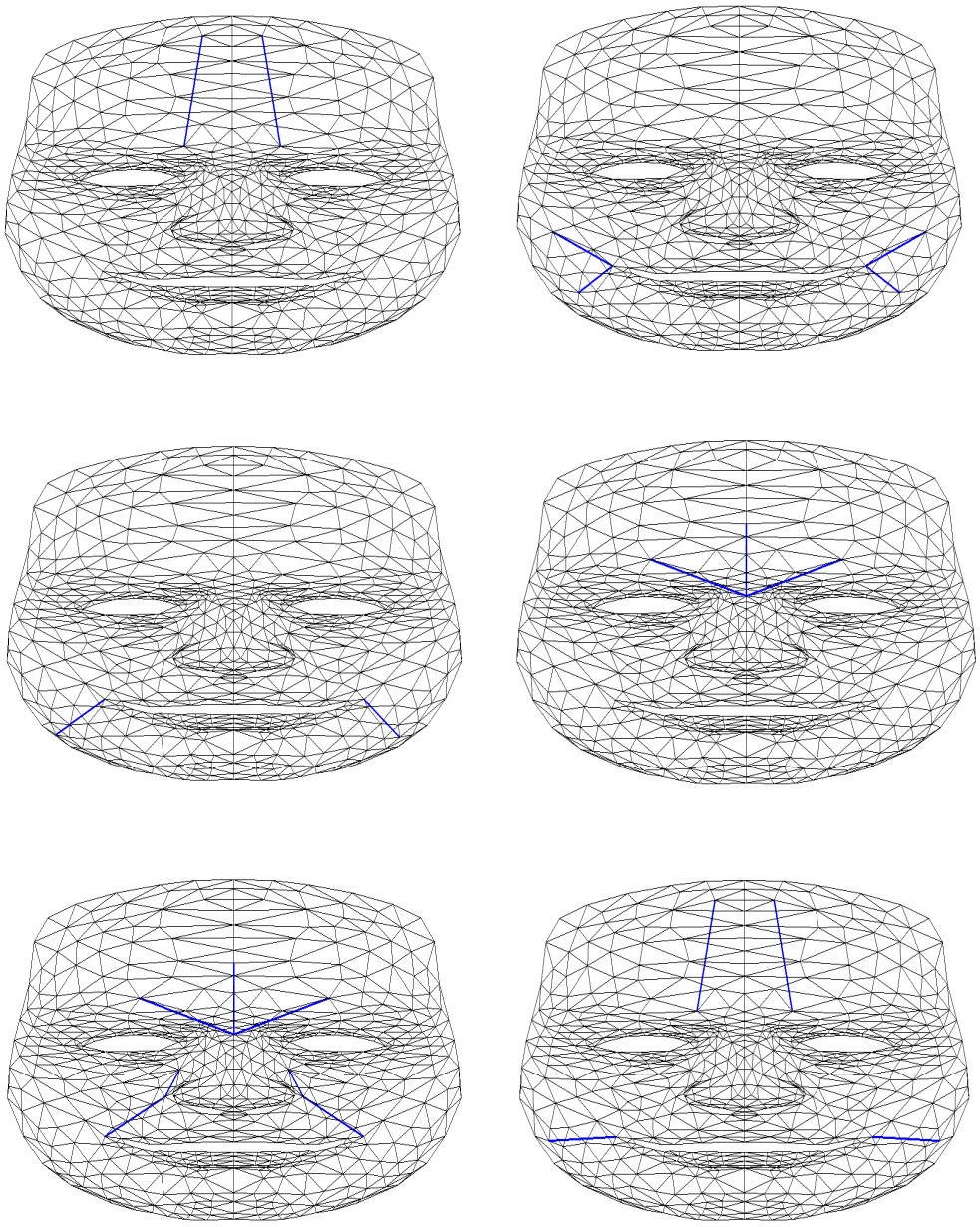

Table 5.3: Facial expressions Surprise, Happy, Sad, Anger, Disgust and Fear are presented respectively.

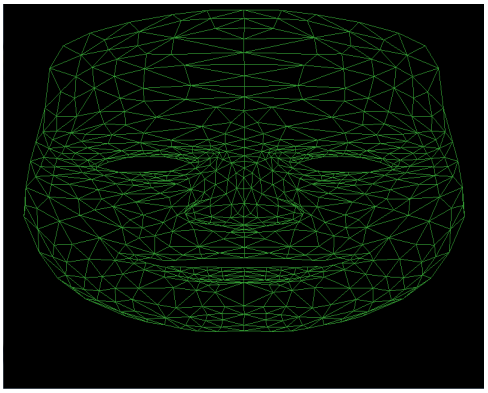

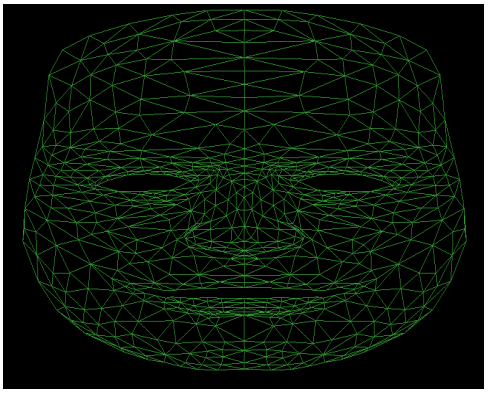

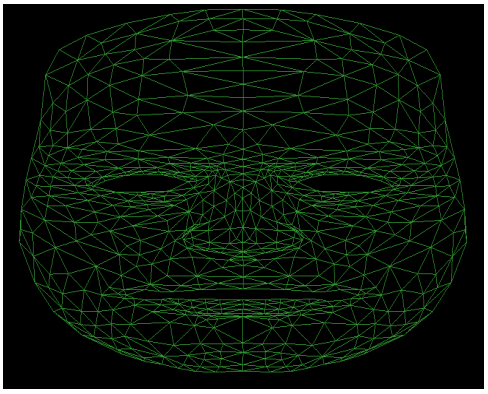

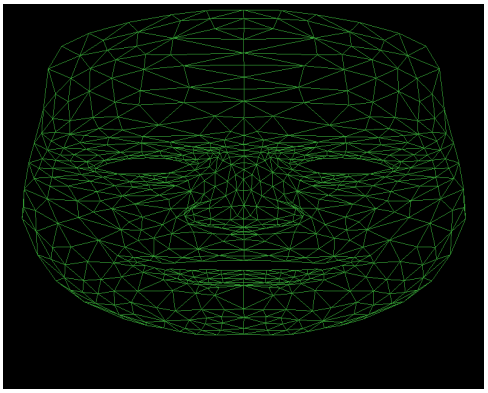

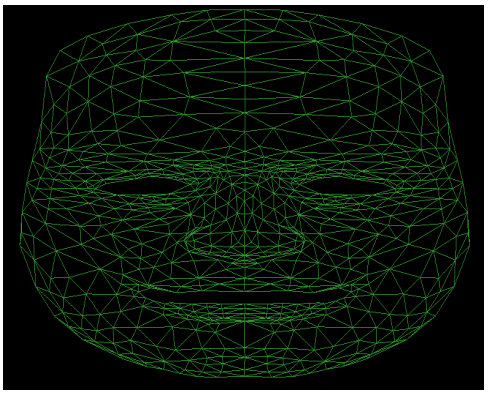

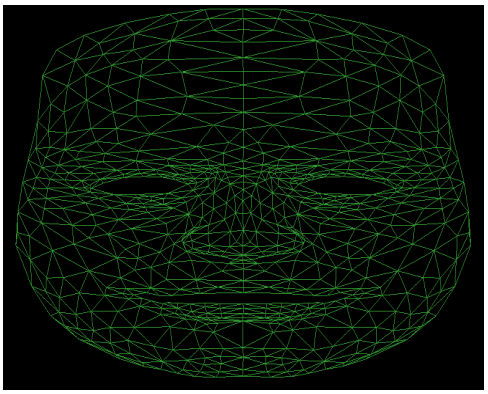

Chapter 6

Conclusion

Face models embed prior information, hence they are frequently used in facial expression simulation and expression studies. The state-of-the-art in face models may include minute details on the structure of the face. Muscle models are often incorporated into generic face models and they define the mechanism of facial expression. Current muscle models are built through trial and error with the aim of producing more realistic simulations. For that reason, they do not necessarily conform with the physical characteristics of muscles.

In this study we derive an anatomical muscle model solely through unintrusive observation of facial expressions. The actual muscle forces are computed using experimental data on skin stiffness and displacement of skin points during performance of an expression. Using the actual force data, we propose a new and realistic muscle model. Comparative analysis of this anatomical muscle model with the state-of-the- art reveals that the proposed model produces more realistic distribution of muscle forces on the facial skin.

The aim of our research is to describe a novel muscle model using actual muscle forces exerted on the facial skin during generation of an expression. We show that muscle force distribution generated by the anatomical muscle model conforms better to the actual physical forces. We show the behavior of skin during generation of an expression. During expression, the stiffness value of skin is not uniform

distribution in region of influence on face and this stiffness value is expressed as piecewise. So we describe a skin model which based on Figure 2.2. According to result, we say that muscle force distribution generated by the anatomical muscle model conforms better to the actual physical forces. We show our result with simulation as shown in the Figure 5.3.

There are many works in this field which deal with different muscle models [15], [14]. These models are found through trial and error. The muscle model that we propose is done in a different way to tracking of points. Firstly, the subject faces were drawn with grids and were asked to make gestures from [table 5.1]. To find muscle force, we are working with only the last frame and the first frame of video. We identify the projected wireframe vertices in the first frame and the last frame we manually mark the new locations of these points. We extract external force on the skin rely on displacement of these points and as we show in 3D plot Figure 5.6.

To extract force, the completion time of the this process can be long. However, the goal of this work obtaining more accurate and more realistic models. Moreover this analysis will be done only once to derive an accurate muscle model. Therefore, time is not significant factor for this research.

Appendix

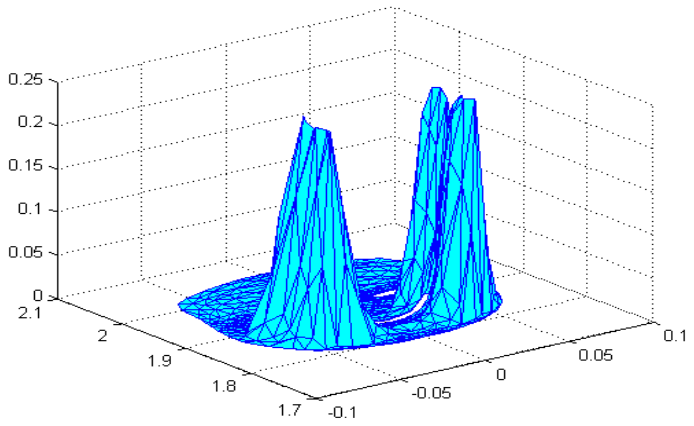

Figure 6.1: Happy expression occurs under the influence of more than two muscles

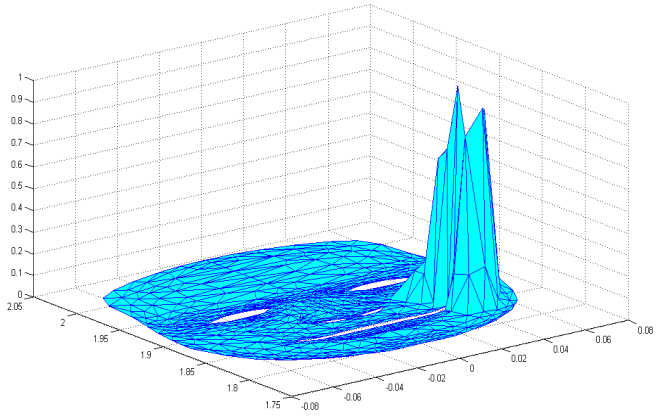

Figure 6.2: Fear expression does not give a clear result

References

[1] A. Mehrabian, "Communication without words," *Psychol. Today*, vol. 2, no. 9, pp. 52–55, 1968.

[2] J. Bulwer, *Philocophus*. EEBO Editions, ProQuest, 1648.

[3] G. de Boulogne and R. Cuthbertson, *The Mechanism of Human Facial Expression*, ser. Studies in Emotion and Social Interaction. Cambridge University Press, 1862/1990.

[4] C. Darwin, *The Expression of the Emotions in Man and Animals*, anniversary ed., P. Ekman, Ed. Harper Perennial, 1872/2009.

[5] P. Ekman and W. V. Friesen, *Pictures of facial affect*. Consulting Psychologists Press, 1976.

[6] M. Stewart, M. S. Bartlett, P. A. Viola, T. J. Sejnowski, B. A. Golomb, J. C. Hager, and P. Ekman, "Classifying facial action," *IEEE Trans. Pattern Anal. and Mach. Intell.*, vol. 21, pp. 974–989, 1999.

[7] H. P. Abeysundera, K. S. Benli, and M. T. Eskil, "Nearest neighbor weighted average customization for modeling faces," *Mach. Vision and Appl.*, vol. 24, no. 7, pp. 1525–1537, 2013.

[8] T. F. Cootes, C. J. Taylor, D. H. Cooper, and J. Graham, "Active shape models-—their training and application," *Comput. Vis. Image Underst.*, vol. 61, no. 1, pp. 38–59, Jan. 1995.

[9] T. F. Cootes, G. J. Edwards, and C. J. Taylor, "Active appearance models," *IEEE Trans. Pattern Anal. Mach. Intell.*, vol. 23, no. 6, pp. 681–685, Jun. 2001.

[10] R. Yang and Z. Zhang, "Model-based head pose tracking with stereovision," in *Fifth IEEE international conference on automatic face and gesture recognition*, May 2002, pp. 255–260.

[11] Y. Lee, D. Terzopoulos, and K. Waters, "Realistic modeling for facial animation," in *Proceedings of the 22Nd annual conference on computer graphics and interactive techniques*, ser. SIGGRAPH '95. New York, NY, USA: ACM, 1995, pp. 55–62.

[12] M. Proesmans and L. Van Gool, "Reading between the lines–a method for extracting dynamic 3d with texture," in *Proceedings of the ACM Symposium on Virtual Reality Software and Technology*, ser. VRST '97. New York, NY, USA: ACM, 1997, pp. 95–102.

[13] E. Sifakis, I. Neverov, and R. Fedkiw, "Automatic determination of facial muscle activations from sparse motion capture marker data," *ACM Trans. Graph.*, vol. 24, no. 3, pp. 417–425, Jul. 2005.

[14] K. Waters, "A muscle model for animating three-dimensional facial expression," in *Proceedings of the 14th annual conference on computer graphics and interactive techniques*. New York, NY, USA: ACM, 1987, pp. 17–24.

[15] R. M. Koch, M. H. Gross, and A. A. Bosshard, "Emotion editing using finite elements," in *Comput. Graph. Forum*, vol. 17, no. 3, 1998, pp. 295–302.

[16] T. Bui, D. Heylen, M. Poel, and A. Nijholt, "Exporting vector muscles for facial animation," in *Smart Graphics*, ser. Lect. Notes Comput. Sc., A. Butz, A. Krüger, and P. Olivier, Eds. Springer Berlin Heidelberg, 2003, vol. 2733, pp. 251–260.

[17] Y. Zhang, E. C. Prakash, and E. Sung, "A new physical model with multilayer architecture for facial expression animation using dynamic adaptive

mesh," *IEEE Trans. Vis. Comput. Graph.*, vol. 10, no. 3, pp. 339–352, May 2004.

[18] Y. Zhang, E. C. Prakash, and E. S., "Face alive," *Journal of Visual Languages & Computing*, vol. 15, no. 2, pp. 125 – 160, 2004.

[19] J. S.-S. Tang, A. W.-C. Liew, and H. Yan, "Human face animation based on video analysis, with applications to mobile entertainment," *J. Mob. Multimed.*, vol. 1, no. 2, pp. 133–148, Jun. 2005.

[20] K. Yano and K. Harada, "A facial expression parameterization by elastic surface model," *Int. J. Comput. Games Technol.*, vol. 2009, pp. 2:1–2:11, Jan. 2009.

[21] Q. Chen, M. D. Cordea, E. M. Petriu, A. R. Varkonyi-Koczy, and T. E. Whalen, "Human computer interaction for smart environment applications using hand gestures and facial expressions," *Int. J. Adv. Media Commun.*, vol. 3, no. 1/2, pp. 95–109, Jun. 2009.

[22] W. Wang, X. Yan, Y. Xie, J. Qin, W.-M. Pang, and P.-A. Heng, "A physically-based modeling and simulation framework for facial animation," in *Fifth international conference on image and graphics*, Sept 2009, pp. 521–526.

[23] Y. Fung, *Biomechanics: mechanical properties of living tissues*, ser. Biomechanics / Y. C. Fung. Springer-Verlag, 1981.

[24] R. Kenedi, T. Gibson, J. Evans, and J. Barbenel, "Tissue mechanics," *Phys. Med. Biol*, vol. 20, no. 5, pp. 699–717, 1975.

[25] M. Rydfalk, "Candide, a parameterized face," Linkping University, Dept. of Electrical Engineering, Sweden, Tech. Rep. LiTH-ISY-I-866, 1987.

[26] J. Ahlberg, "Candide-3, an updated parameterized face," Linkping University, Dept. of Electrical Engineering, Sweden, Tech. Rep. LiTH-ISY-R-2326, 2001.

[27] D. Terzopoulos and K. Waters, "Physically-based facial modelling, analysis, and animation," *J. Visual. Comp. Animat.*, vol. 1, no. 2, pp. 73–80, 1990.

[28] Y. Luximon, R. Ball, and L. Justice, "The 3D chinese head and face modeling," *Comput. Aided Des.*, vol. 44, no. 1, pp. 40–47, Jan. 2012.

[29] T. Erkoc, "Anatomy based animation of facial expressions," Master's thesis, University of ISIK, Turkey, 2013.

[30] E. Goldfinger, *Human Anatomy For Artists*, ser. The Elements of Form / E. Goldfinger. Oxford University Press, 1991.

[31] Y. Zhang, E. Sung, and E. Prakash, "Adaptive simulation of facial expressions," in *IEEE international conference on multimedia and expo*, Aug 2001, pp. 865–868.

Curriculum Vitae